Rev.Adv.Mater.Sci. 2 (2001) 44-79

DISCLINATIONS IN LARGE-STRAIN PLASTIC DEFORMATION AND WORK-HARDENING

M. Seefeldt

Catholic University of Leuven, Department of Metallurgy and Materials Engineering, Kasteelpark Arenberg 44, B-3001 Heverlee, Belgium

Received: September 01, 2001

Abstract. Large strain plastic deformation of f.c.c. metals at low homologous temperatures results in the subdivision of monocrystals or polycrystal grains into mesoscopic fragments and deformation bands. Stage IV of single crystal work-hardening and the substructural contribution to the mechanical anisotropy emerge at about the same equivalent strain at which the fragment structure becomes the dominant substructural feature. Therefore, the latter is likely to be the reason for the new features in the macroscopic mechanical response. The present paper reviews some experimental and theoretical work on deformation banding and fragmentation as well as a recent model which tackles the fragment structure development as well as its impact on the macroscopic mechanical response with the help of disclinations. Incidental or stress-induced formation of disclination dipoles and non-conservative propagation of disclinations are considered as "nucleation and growth" mechanisms for fragment boundaries. Propagating disclinations get immobilized in fragment boundaries to form new triple junctions with orientation mismatches and thus immobile disclinations with long-range stress fields. The substructure development is described in terms of dislocation and disclination density evolution equations; the immobile defect densities are coupled to flow or critical resolved shear stress contributions.

1. INTRODUCTION

The activation of *rotational modes of deformation*, i.e. the *spatially and temporally progressing* reorientation of parts of monocrystals or polycrystal grains in the course of plastic deformation, and its impact on the macroscopic mechanical response were intensively studied in Physical Metallurgy since the 1930s. The phenomenon was discovered through X-ray diffraction at deformed metals exhibiting *Laue asterism*, i.e. a subdivision of the ideal Bragg reflexes into sets of subreflexes, corresponding to the subdivision of grains into sets of subgrains.

Monocrystal or grain subdivision was studied in a variety of different contexts: In the early years of Physical Metallurgy, deformation banding, especially kink banding, was studied in order to understand *kinking* as an additional *mechanism of plastic deformation* next to dislocation gliding and deformation twinning [1,2] (and next to grain boundary gliding and deformation-induced phase transformations which were discovered later). With the new possibilities of transmission electron microscopy (TEM) in the 1960s the attention of metal physicists was drawn to individual dislocation behaviour in the early stages of plastic deformation. However, deformation banding was rediscovered in *texture research* where the disregard of *grain subdivision* was understood to be one reason for the deficiencies in texture prediction, especially in *local texture prediction*.

Already at the beginning of the 1960s monocrystal subdivision on a smaller scale than the one of the deformation bands was discovered in TEM: *misorientation bands* were found, a *band substructure* arising during stage III of work-hardening. Extensive TEM studies in the 1970s and 1980s revealed deformation banding on the II. mesoscopic scale and fragmentation on the I. mesoscopic scale to be *the* characteristic features of the substructure development at intermediate and large strains, in the *developed stage of plastic deformation*, as Rybin phrased it. At the same time, the stages IV and V of work-hardening as well as the substructural contribution to the mechanical anisotropy were discovered. However, only in Russia it was tried from the beginning to connect these new features in the

Corresponding author: M.Seefeldt, e-mail: Marc.Seefeldt@mtm.kuleuven.ac.be

macroscopic mechanical response to the new features in the substructure evolution, namely to fragmentation. Still today, the connection between stage IV and fragmentation is not yet generally accepted, neither on experimental nor on theoretical grounds.

This development was also driven by technological interest: All the industrially relevant forming processes, as, for example, flat rolling, deep drawing or wire drawing, involve large strains, high strain rates and multiaxial deformation modes. Recently, the production of ultra-fine grained and bulk nanostructured materials by means of severe plastic deformation – which is essentially based on extensive fragmentation – found increasing interest also in industry.

This section gives a brief overview on deformation banding and fragmentation and large strain work-hardening – the framework within which the present work is situated. The *second section* explains the concepts of reaction kinetics and disclinations used in the proposed model – the approach or point of view taken by the present work. The *third section* presents a semi-phenomenological application to the cell and fragment structure development and their impact on the flow stress for single crystals with symmetric orientation. The model is capable of reproducing stages III and IV of the room temperature work-hardening curve for copper.

1.1. Deformation banding and fragmentation

Since the 1930s and extensively in the 1950s light and electron microscopy studies of slip line patterns and X-ray studies of Laue asterism were used to investigate deformation banding during plastic deformation. In most cases, aluminium single crystals after tensile deformation at room temperature were studied. Barrett and Levenson [3,4] used macroscopic etching methods to reveal orientation differences and found band-shaped surface structures. They defined a *deformation band* as a region in which the orientation progressively rotates away from that in the neighbouring parts in the crystal and suggested that "deformation bands form as a result of the operation of different sets of slip systems in different band-shaped regions".

Honeycombe [5,6] distinguished, based on optical microscopy surface studies and X-ray asterism measurements at aluminium single crystals, two types of bands: a) *kink bands* are narrow bent regions (typically with *double* curvature) normal to the active slip direction which separate slightly disoriented crystal lamellae, and b) *bands of secondary slip* are regions nearly free of primary slip traces and almost parallel to the primary slip planes in the early stages of plastic deformation. The influence of the crystal orientation, the temperature, the deformation speed and the crystal purity was studied. The essential feature of the kink bands is the *bending* which gives rise to a diffuse, streak-like Laue asterism. The bands of secondary slip act as preferential sites of activation of unexpected slip systems and thus also exhibit disorientations, but they are essentially free of curvature.

Kink bands were almost absent in deformed crystals with highly symmetric initial *orientations* (deforming through conjugate slip on two or more slip systems from the beginning) and were most pronounced in crystals with initial orientations close to the centre of the standard triangle of the stereographic projection (deforming mainly through primary slip). Bands of secondary slip were observed for all initial orientations, but were most pronounced and even of macroscopic size in multiple-slip oriented crystals (deforming through conjugate slip e.g. on four active systems). Kink bands were observed in a wide range of *temperatures*. However, the spacing between the bands turned out to be about 2-3 times larger at high temperatures and too small for observation with optical microscopy at liquid nitrogen temperature. At temperatures above 450 °C, polygonization of the bent regions was observed, resulting into a sharp, small spot-like Laue asterism. The influence of the deformation speed on both types of banding was found to be small.

From recovery experiments [6], it was concluded that the Laue asterism was due to *deformation-induced* banding. Honeycombe [5] attributed the formation of kink bands to the restraints imposed by the grips on the crystals. In case of multiple slip, the stresses due to these restraints could be reduced by slip on alternative slip systems. The formation of bands of secondary slip was ascribed to unpredicted cross-slip at the beginning of plastic deformation which could hinder slip on primary slip systems. So as early as 1951 two different types of deformation banding were distinguished and traced back to two different reasons, namely to an *imposed* one on the *macroscopic* scale – the restraints owing to the deformation mode – and to an *intrinsic* one on the *microscopic* scale – dislocation dynamics leading to unexpected cross-slip.

Staubwasser [7] used surface slip line and X-ray asterism studies on aluminium single crystals after tensile deformation at room and liquid air tem-

perature in order to investigate the orientation dependence of excess dislocation boundary and kink band formation and work-hardening. Low-symmetric single-slip orientations in the lower central part of the standard triangle showed strong asterism right from the beginning of plastic deformation, corresponding to the formation of excess dislocation tilt boundaries perpendicular to the glide direction. With increasing deformation, strong kink-banding was found, also perpendicular to the glide direction and with net misorientation across the band. High-symmetric multiple-slip orientations, on the contrary, exhibited only weak asterism, corresponding to the formation of dislocation walls perpendicular to all of the active slip planes. No kink-banding at all was observed. Furthermore, Staubwasser suggested a mechanism for kink band formation. Groups of primary dislocations could get stopped at (unspecified) obstacles, and *"such on neighbouring planes could be held fast by the former ones"*. The arising excess dislocation boundaries were still penetrable to mobile dislocations. However, at the end of stage I, the stress fields around the dislocation boundaries would activate a secondary slip system, so that immobile barriers could be formed through dislocation reactions. Mobile dislocations would then pile up at the now intransparent boundaries and induce the characteristic *S*-shaped lattice curvature of the kink bands. Fully developed kink bands would then be impenetrable obstacles and have a serious impact on work-hardening.

Mader and Seeger [8] distinguished, based on replica studies of slip lines patterns on copper single crystals deformed at room temperature, two different types of kink bands: the kink bands of the first type arise already at the end of stage I and mainly in stage II, are of macroscopic size (length between several 100 μm and the specimen size, width between 10 and 100 μm) and are very straight. The kink bands of the second type arise at the beginning of stage III, are of mesoscopic size (only about 100-200 μm long and very narrow) and are less straight, a bit wavy and connected to each other through branches. They correspond to the misorientation bands on the mesoscopic scale studied later on in TEM. The present paper focusses on these misorientation bands on the (first) mesoscopic scale rather than on the kink and deformation bands on the grain-size or (second) mesoscopic or even macroscopic scale.

In the early TEM era at the beginning of the 1960s, Steeds [9] and Essmann [10] investigated the dislocation arrays in single-slip oriented copper monocrystals after tensile deformation at room temperature. At the beginning of stage III, they found flat, *disk-shaped areas parallel to the primary slip planes* which were limited by secondary dislocations and included long bowed-out primary dislocations, but only *few* forest dislocations. According to Essmann, the disks were *misoriented* by 0.2-1.0° with respect to each other and the boundaries had a mixed tilt-twist character. He drew a remarkable conclusion from a comparison of Steeds' and his micrographs: while both of them agreed on the disk structure parallel to the primary slip planes, their statements on the height of the disks varied: Steeds found 1-2 μm, Essmann 0.4 μm. Following Essmann, Steeds' result matched with the period of the *large misorientations* which he also observed, but found to be *subdivided on a finer scale*. In spite of these early TEM findings of a *misorientation band substructure*, the attention of metal physicists was then mainly drawn to the dislocation structures in the stages I and II of work-hardening, especially to individual dislocations, Lomer-Cottrell barriers, pile-ups, dislocation bundles and cell walls (for an overview see e.g. [11]).

However, in the mid 1960s, deformation banding and fragmentation were rediscovered in another context, namely in texture research. A long-standing problem in this field was the mechanism for the formation of a <111> and <100> double fibre texture in wire-drawing of f.c.c. metals. Ahlborn [12,13] studied the orientation development of f.c.c. single crystals (Ag, Au, Cu, Al, brass) during wire-drawing using the X-ray rotation crystal method. He found the single crystals to split up into deformation bands with volume fractions of the two components strongly varying among the metals. He connected this variation to the variation in stacking fault energy. Later on, Ahlborn and Sauer [14] used TEM to study deformation banding on the (second) mesoscopic scale as well as fragment and cell structure development on the (first) mesoscopic and microscopic scales at copper single crystals during wire-drawing. The extensive TEM study by Malin and Hatherly [15] also aimed at a better understanding of the coupling between fragmentation, deformation banding and texture evolution.

In line with Essmann's remark, Likhachev, Rybin and co-workers were the first to distinguish between the *cell structure* development on the *microscopic scale* and the *fragment structure* development on the *(first) mesoscopic scale* [16-18]. The cell structure development, as reflected in the average cell size, cell wall width or misorientation across cell

walls, was found to be very slow at large strains, so that Rybin [18] called the cell structure *"frozen"* [1].

Therefore, *large-strain plastic deformation* and *work-hardening* were ascribed to the *fragment structure evolution*. Fragmentation was recognised as an almost universal phenomenon which takes place in f.c.c., b.c.c., and h.p. mono- as well as polycrystalline metals and alloys. Cell sizes, fragment sizes as well as orientations and misorientations of fragment boundaries were measured mainly at molybdenum (as a representative for the b.c.c. materials) mono- and polycrystals but also at nickel (for the f.c.c. materials) and α-titanium (for the h.p. materials) [17,18]. The St. Petersburg school of plasticity interpreted the arising *fragment boundary mosaic* as a *network of partial disclinations* in the mosaic's triple junctions [16,20,21] and ascribed *fragmentation* to the elementary processes of *generation*, *propagation* [18,22,23] and *immobilization of partial disclinations* (see below).

Hansen, Juul Jensen, Hughes and co-workers studied grain subdivision mainly in pure aluminium [24-28] and nickel [25,26,29-31] but also in Ni-Co and Al-Mn alloys [25,29] as well as in copper [32]. Cold-rolling [24-28,30,32] as well as torsion [25,29,30] were applied. Recently, single crystal fragmentation was investigated in pure aluminium after channel-die compression [33,34] and cold-rolling [35]. The cell and cell block sizes as well as the wall and boundary orientations and misorientations were characterized extensively. Whereas the cell size and the misorientation across cell walls (CW) remain almost constant at large strains, the cell block size continues to decrease, and the misorientation across the cell block boundaries (CBB) continues to increase. The cells are roughly equiaxed, while the cell blocks are elongated and show a strong «directionality». The CW were interpreted as «incidental dislocation boundaries» (IDB), the CBB as «geometrically necessary boundaries» (GNB). Both of them are considered as low energy dislocation structures (LEDS). Especially, the interpretation of the CBB as Frank boundaries free of long-range stresses turned out to correspond with TEM results [36]. According to the Risø school, fragmentation is due to the activation of different sets of locally less than five slip systems (giving lower densities of intersecting dislocations and thus of jogs) [25] or due to different slip rates within the same set of active slip systems [36].

Recently, the orientation dependence of grain subdivision was investigated. In a TEM study on cold-rolled aluminium polycrystals, Liu et al. [28] classified the subdivision patterns into three types: Type A^{I} grains (mainly near the Goss and S texture components) split up into a quite uniform cell block structure with crystallographic boundaries parallel to the active {111} slip planes. Type A^{II} grains (scattered) split up into a non-uniform structure with crystallographic boundaries. Type *B* grains (roughly around the cube type texture components) split up with non-crystallographic boundaries and on two different scale levels, on the (first) mesoscopic one and on the grain-size or (second) mesoscopic one. The latter probably corresponds to deformation banding in cube-oriented single crystals. The subdivision patterns of channel-die compressed and cold-rolled, respectively, aluminium single crystals with the brass, the copper and the cube orientation were discussed in [33-35].

To the author's knowledge, Koneva, Kozlov and co-workers [38-42] were the first

- to distinguish two nucleation mechanisms for fragmentation, namely an intrinsic one and a grain boundary-induced one and
- to distinguish the discrete misorientations across the fragment boundaries and continuous misorientations bending and twisting the fragment interiors (for a scheme, cf. Fig. 1).

Their conclusions were based on TEM studies of compressed f.c.c. Cu-, Ni- and Fe-based alloys in the long-range and short-range ordered solid solution states.

According to Koneva, Kozlov and co-workers, the beginning of *stage* III is characterized by the emergence of terminating as well as continuous dislocation boundaries with *discrete misorientations*. These boundaries appear in *band-like configurations* made up of parallel boundaries which rotate the lattice inside the band with respect to the matrix (and grow in band direction) as well as *in loop-like configurations* made up of a closed boundary ring (see and in Subsection 3.2.3. below) which rotates the loop interior with respect to the matrix (and grows perpendicular to the loop). The different configurations are the result of different nucleation mechanisms:

[1] This steady state of the cell structure is a dynamic one: Dislocations would constantly get trapped into and emitted from the cell walls. However, there is experimental evidence [19] that at least in copper cell refinement is realised by cell subdivision rather than by cell wall motion. Strictly speaking, the *geometry* of the cell structure is frozen in the steady state, but not the cell structure itself.

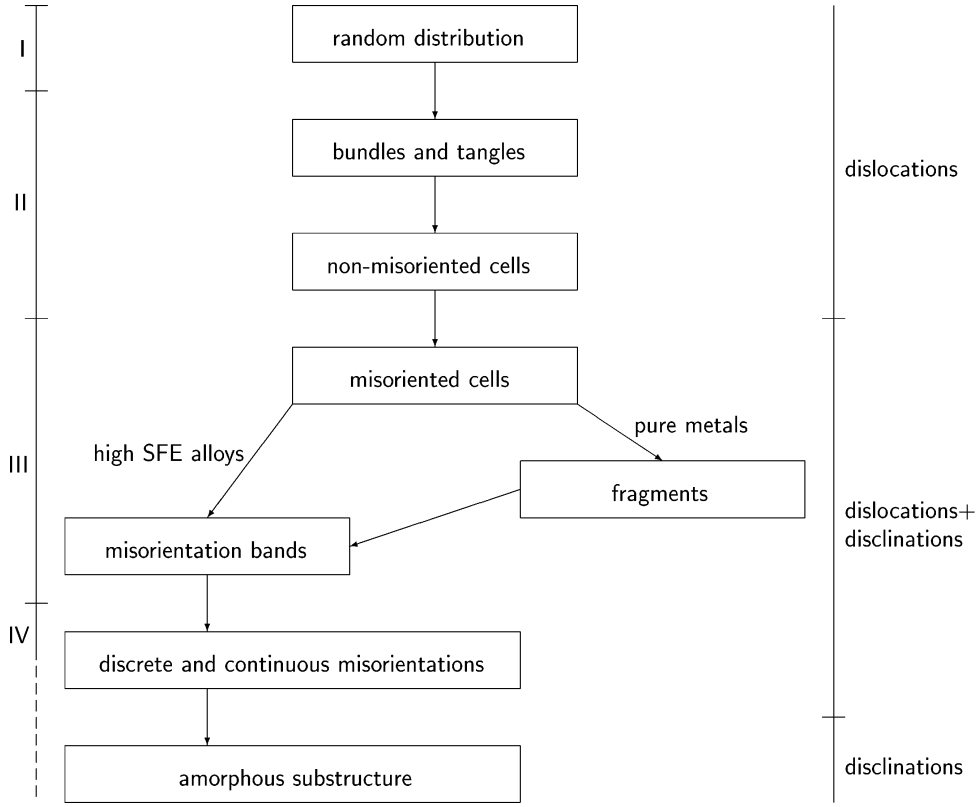

Fig. 1. Schematic representation of substructure development under plastic deformation at low homologous temperatures or without signifcant influence of diffusion. Simplified and slightly modified after Kozlov, Koneva and coworkers ([40], p. 96).

- grow of band systems from polycrystal grain boundaries, especially from steps in the grain boundaries and
- nucleation and development of closed subboundary rings bordered by partial disclination loops.

Which of the mechanisms operates, depends, for instance, on the previous substructure and on the presence of grain boundaries. Both mechanisms lead to a misorientation band substructure with first one and later two or more intersecting band sets which gradually cover the whole volume of the specimen. At the beginning of stage III, the sets were oriented parallel to non- or only slightly active octahedral slip planes and were either of a pure tilt or pure twist character. With increasing deformation, the sets deviated more and more from the octahedral slip planes and were of a mixed tilt-twist character. In *stage* IV, the misorientation band substructure is present in the whole specimen volume. Beyond that, *continuous misorientations* with small but increasing orientation gradients develop *inside* the misorientation bands due to local *bending and twisting*. At the beginning of stage IV, mostly either pure bending or pure twisting was found. At larger deformations, distortions of a mixed type predominated.

Kozlov, Koneva and co-workers used the following quantities to characterize the substructure: the redundant[1] (or “incidentally stored” or “scalar”) dislocation density ρ_r and the non-redundant or excess (or “geometrically necessary” or “tensorial”) dislocation density ρ_{exc}, the subboundary spacing d_f, the radial and azimuthal subboundary misorientations ω_{rad} and ω_{az}, the lattice curvature or lattice bend twist κ. The non-redundant dislocation density ρ_{exc} was calculated as the density of dislocations accommodating *lattice rotation mismatches* through dividing the lattice rotation difference by the bending extinction contour width l

$$\rho_{exc} = \frac{\kappa}{b} = \frac{\Delta\varphi}{l}. \qquad (1)$$

While the growth rate of the redundant dislocation density was maximum in stage II, the one of the non-redundant dislocation density was maximum

[1] The distinction between redundant and non-redundant dislocations was introduced by Weertman [37].

in stage III. It was observed that extensive generation of non-redundant dislocations starts at a critical redundant dislocation density of about 1.5 - $3 \cdot 10^{14}$ m^{-2}. Plotting the mean misorientation ω and the average lattice curvature κ over the redundant dislocation density ρ_r clearly revealed the transition from stage III to stage IV. The results can be summarized in the scheme presented in Fig. 1 taking pattern from Kozlov et al. [40].

Continuous and discrete misorientations were also distinguished and analysed quantitatively in a recent OIM study at cold-rolled aluminium AA1050 by Delannay et al. [43]. The subdivision of each grain was characterized by measuring the orientation spread within the grains. Two parameters were defined: the average misorientation of all grid points within one grain with respect to the mean orientation of that grain (reflecting a large orientation spread across the grain), and the average misorientation between neighbouring grid points in the orientation map (reflecting the subdivision into highly misoriented fragments). Both parameters were calculated separately for each grain. It was concluded that grains with orientations close to cube have higher orientation spreads than grains along the β-fibre. Furthermore, among the grains with a strong lattice distortion, only those with orientations close to copper and TD-rotated cube (cube rotated by 22.5 ° around the transverse direction) have high neighbouring-points misorientations.

The models which were proposed to describe and explain fragmentation, can roughly be grouped into two families. The first family is based on *texture-type* approaches. These models start from either different sets of active slip systems or different slip rates within the same set of active systems in different crystal parts (see, for instance, [44-47]). However, in general they lack an explanation for the initiation of the fluctuations in the slip regime. The second family is based on *nucleation and growth* approaches. These models discuss the generation of short segments of fragment boundaries and the conditions for their growth. The arising fragment boundaries then *impose* the variations in the slip regime. However, the models in this family usually fail in describing the transition from a homogeneous to an inhomogeneous slip regime quantitatively, i.e. they fail in treating the fragments as separate texture components starting from a certian critical misorientation.

Considering any inhomogeneous slip regime, it has to be emphasized that compatible deformation of all crystal parts has to be ensured, so that spatially varying sets of slip rates may only result in varying lattice rotation rates but not in varying strain rates, i.e. they have to be different solutions of the same Taylor problem. The Risø school proposed the selection of different sets of less than five active slip systems in different cell blocks because with fewer active slip systems less dislocation jogs have to be produced and less energy is dissipated [25]. The selection of different sets of active slip systems results in different lattice rotation rates and thus requires the formation of geometrically necessary boundaries to accommodate the lattice rotation mismatch and to separate the evolving cell blocks from each other. Dislocation dynamics has to provide the dislocations to construct these boundaries.

In this approach the choice of different sets of active slip systems is thus prior to the formation of the geometrically necessary boundaries. This would require spontaneous collective behaviour of dislocations in a mesoscopic volume which is not likely to occur. Supposing that local dislocation dynamics is controlled only by the locally present stress fields.

In the author's opinion, fragmentation should be triggered off by *local* rather than *global* slip imbalances across an obstacle. This results in the generation of a both-side terminating excess dislocation wall which can be completed to form a both-side terminating small-angle grain boundary as a nucleus of a misorientation boundary which would then, with the help of its long-range stress fields, *impose* different slip rates. In this approach, the nucleation and growth of a misorientation boundary would thus be prior to the choice of different sets of slip rates. In the framework of the model to be discussed in this paper, the nucleation and growth of fragment boundaries is only possible in the combination of bundling of mobile dislocations in slip bands and of stochastic trapping in a semi-transparent obstacle.

1.2. Large strain work-hardening

The coupling between the macroscopic mechanical properties of a material and its micro- and mesoscopic structure is the key to the development of new materials with high strength and good formability. Since all the industrially relevant forming processes as, for instance, flat rolling, deep drawing or wire drawing, involve intermediate and large strains, a better understanding of the coupling between work-hardening and substructure development is strongly desirable especially for intermediate and large strains.

The substructural background of the transition from stage III to stage IV of work-hardening is still a matter of controversial discussion. What all stage IV models have in common is the use of (at least) two substructural variables, mostly dislocation densities, as suggested by Mughrabi [48] for any model considering substructure development and work-hardening at intermediate and large strains. The early stage IV models [49-52] started from a dislocation cell structure, treated it as a compound made up of the cell interiors as a «soft phase» and of the cell walls as a «hard phase» [48,53], used the cell interior and cell wall dislocation densities as substructural parameters and ascribed the shear resistances of the two phases to the respective local dislocation densities. The ideas on the underlying dislocation kinetics varied. It was noticed that the low hardening rate of stage IV was rather close to the one of stage I of single crystal plasticity and suggested that the underlying elementary processes should also be related to each other (see e.g. [54]). In line with this assumption, Prinz and Argon [49] proposed the formation of hardly mobile dislocation dipoles in the cell interiors and their drift to the cell walls to be the rate-controlling mechanism of stage IV. Haasen [51] and Zehetbauer [52], on the contrary, were prompted by different features of stage IV in low and high temperature deformation to focus on the different storage and recovery mechanisms of screw dislocations in the cell interiors and of edge dislocations in the cell walls. The model by Zehetbauer [52] took the concentration of plastic vacancies as an additional substructural variable into account. With four fitting parameters (which could quantitatively be interpreted on physical grounds), it was able to reproduce work-hardening curves for a variety of different temperatures in excellent agreement with experiment.

However, the model was based on questionable assumptions concerning the elementary processes and the substructural framework: interactions between screw and edge dislocations were neglected, and experimental evidence of fragmentation (e.g. misorientation bands, cell blocks) as well as of long-range stresses (bow-out of dislocations in the cell interiors in TEM [11,55], asymmetric XRD line broadening [56]) was disregarded. Furthermore, the model predicted substructural features which were in conflict with experimental results: considerable dislocation densities in the cell interiors were predicted, whereas TEM studies in the unloaded as well as in the neutron-pinned load-applied state revealed only very small densities [11,55], and a transition from the screw to the edge dislocation density dominating dislocation kinetics was concluded to cause the transition to stage IV, while recent X-ray studies indicate that such a change in the dominating dislocation character takes place already in stage III [57].

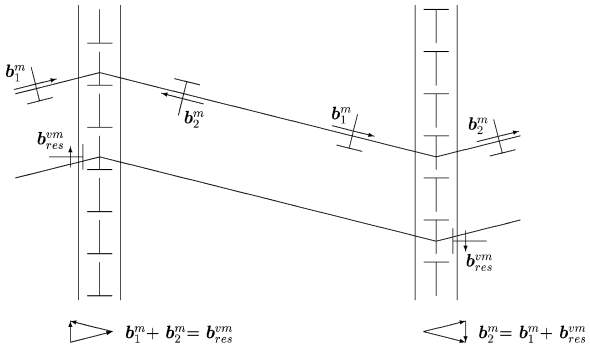

Fig. 2. Generation of "virtual misfit dislocations" by mobile dislocations travelling across misorientation boundaries. To the left, two mobile dislocations of opposite sign which do not fully compensate each other any more and thus leave a "virtual misfit dislocation" behind. To the right, a mobile dislocation penetrating through the boundary leaving a "virtual misfit dislocation" behind.

With the increasing amount of experimental results on grain subdivision it became clear that a substructure-based model of stage IV work-hardening should take fragmentation into account. Haasen [51] had already assumed that different sets of slip systems were active in different cells and causing «geometrically necessary» boundaries between the cells, but Argon and Haasen were the first to model the coupling between increasing misorientation and work-hardening [58]. They ascribed the stage IV work-hardening rate to the fact that dislocations of opposite signs, approaching a misorientation boundary from the two adjacent fragments, do not fully compensate each other any more. Consequently, elastic misfit stresses accumulate, or, in defect language, "virtual misfit dislocations" with a "Burgers vector" equaling the difference of those of the two dislocations from the two sides (see Fig. 2). These elastic stresses or "virtual misfit dislocations" were translated into an organized shear resistance of the cell interiors. The misorientation was first assumed to accumulate with the square root of the shear strain, $\varphi = B\sqrt{\gamma}$. Nabarro [59] proposed the coefficient B to scale with the inverse square root of the fragment size,

$$\varphi = \sqrt{\frac{b}{d_f}}\sqrt{\gamma}. \qquad (2)$$

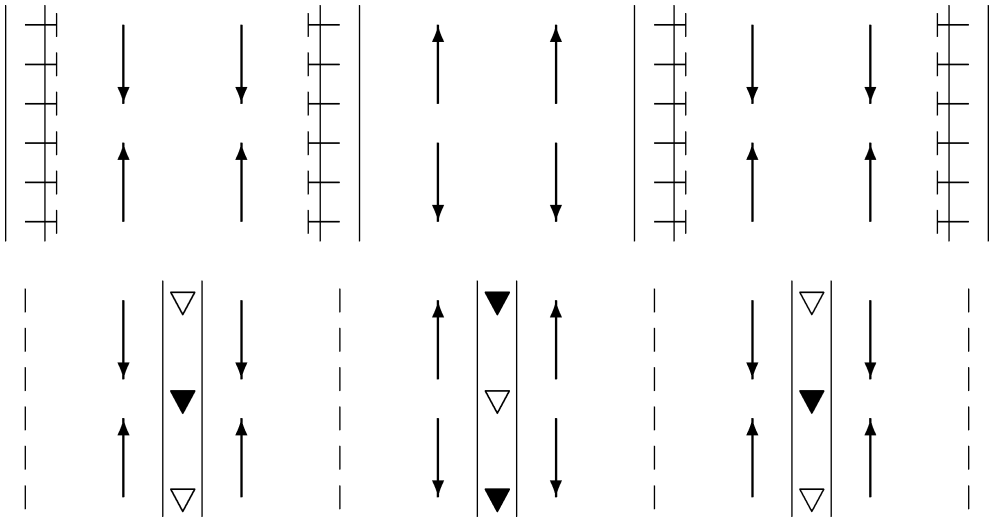

Fig. 3. Above: Argon and Haasen: alternating tensile and compressive misfit stresses due to "virtual misfit dislocations" resulting from mobile dislocations travelling across misorientation boundaries. Below: This work: the misorientation boundary mosaic represented in terms of partial disclinations generating the same pattern of alternating tensile and compressive misfit stresses.

Based on this scaling law, a work-hardening rate of

$$\frac{d\tau_c}{d\gamma} = \frac{8}{3}\frac{B^2 G}{3(1-\nu)}\gamma = \frac{8}{3}\frac{Gb}{(1-\nu)}\frac{\gamma}{d_f} = \frac{8}{3}\frac{G}{(1-\nu)}\varphi^2 \qquad (3)$$

for the shear resistance of the cell interiors was derived.

Argon and Haasen demonstrated that the misfit stresses obtained from their model were compatible with the X-ray residual stress measurements by Mughrabi and coworkers [56] (as one might already guess from the arrangement of "virtual misfit dislocations" in the case of single slip, see Fig. 3, which resembles the arrangement of "interface dislocations" in the case of multiple slip according to Mughrabi [56]). While Mughrabi and coworkers decomposed the asymmetric X-ray peak profiles into two symmetric components and ascribed them to the two "phases" of cell walls and cell interiors (with the peak widths reflecting the respective local dislocation densities and the peak shifts reflecting the respective local residual stresses), Argon and Haasen decomposed them into three symmetric components and ascribed one to the "phase" of cell walls (also with the width reflecting the local dislocation density and the shift reflecting the local residual stress) and the remaining pair of peaks to the "phase" of cell interiors (with the two widths reflecting the alternating tensile and compressive elastic mismatch stresses). An important conclusion from this reasoning was that the decomposition and substructural interpretation of X-ray profiles is not unique. For example, a similar misfit stress distribution as proposed by Argon and Haasen on the basis of "virtual misfit dislocations" can be suggested on the basis of a regular array of partial disclinations describing the mosaic of fragment boundaries (see Fig.3).

However, the mechanism proposed by Argon and Haasen does not distinguish between the cell and the fragment structure. If one applies it to the cell structure, problems arise in case if the cell wall width is of the same order of magnitude as the cell size, as it is typical for substructures evolving during deformation at low homologous temperatures, i.e. without significant influence of diffusion. Mobile dislocations of opposite signs from the two adjacent cells would hardly get into contact with each other, and penetration would more and more replaced by trapping of one dislocation plus emission of another. The consequences on the accumulation of elastic misfit stresses would be unclear and would strongly depend on the cell wall morphology. If one applies it to the fragment structure, the scaling law for the misorientation, Eq. (2) might have to be modified and the coupling with the cell stucture evolution model would get lost.

To the author's knowledge, Koneva, Kozlov and coworkers [38-42] were the first to propose the *excess dislocation density* as the second substructural variable required to describe substructure de-

velopment at intermediate and large strains *and* to couple the increasing excess dislocation density and the increasing misorientation to an additional flow-stress contribution. They suggested

- to connect the transition to stage IV of work-hardening to misorientation bands and fragments becoming the predominant substructural features and
- to consider the excess dislocation density ρ_{exc} as the substructural variable which controls stage IV work-hardening.

In contrast to Argon and Haasen, they did not ascribe this connection to elastic misfit stresses due to the presence of the misorientation boundaries themselves but to the boundaries acting as glide barriers, to *Randspannungen* (end stresses) around the edges of terminating boundaries and to the lattice curvature due to the continuous misorientations in the fragment interiors.

The *kinetics* of band substructure development and of the growth of its volume fraction was observed to be connected to the growth of subboundaries through the material, in the course of which the ratio of the number of terminating subboundaries and of the total number of subboundaries remained constant. The *terminating subboundaries* were identified as *defects of disclination type* on grounds of an analysis of the magnitude and functional decay of the long-range stress fields around them. In the same measure as the non-redundant dislocation density, the long-range stress fields grew. Starting from the middle of stage III, when the volume fraction of the band substructure became significant, the macroscopic flow stress proved to be proportional to the average lattice curvature. The origin of this flow stress contribution was proposed to be closely related to the long-range stress fields. The macroscopic flow stress would then be controlled not only by the local shear resistance due to elastic and contact interaction between the dislocations, but also by the barrier resistance due to the new boundaries and by long-range stresses due to the new excess dislocation configurations. The flow stress was observed to be proportional to

- excess dislocation density,
- subboundary density, and
- misorientation.

Randspannungen (end stresses) were first suggested by Seeger and Wilkens [60] around the edges of terminating boundaries as an additional source of long-range stresses in stage II of plastic defomation, after it had turned out that classical pile-ups were well observed in TEM, but not in sufficient number to explain the stage II work-hardening rate [11]. Later on, they were often mentioned as a possible source of long-range stresses (see, for instance, [29,48]), but, to the author's knowledge, not incorporated into a work-hardening theory so far.

2. MODELLING FRAMEWORK

In the theory of crystal plasticity, plastic deformation and work-hardening are understood as a result of the generation, motion, immobilization and annihilation of point, line and plane crystal defects. These elementary mechanisms are controlled by the external applied stress field as well as by material and process parameters as, for example, stacking fault energy, vacancy formation enthalpy, temperature and deformation speed. A major task of plasticity modelling is to make a choice of defect populations which are relevant under given material and process conditions. This choice should be based on a physical consideration of the dependence of the elementary mechanisms on the material and process parameters (see subsection 2.1). In order to couple the defect populations to the macroscopic behaviour and properties of the material, the volume densities of the point, line and the defects populations are represented by plane defects. A dynamic consideration of plastic deformation and work-hardening then requires a description of the evolution of these densities with time or strain (see subsection 2.2). In a third step, the impact of the stored defects on the local shear resistance and on the long-range internal stresses has to be discussed and the defect densities have to be coupled to critical resolved shear stress or flow stress contributions (see subsection 2.3).

2.1. Materials and processes

In the present paper, the *quasistatic* deformation of f.c.c. metals with *intermediate and high stacking fault energies* at *room temperature* is discussed. In the model presented in section 3, *uniaxial compression* of a *multiple-slip oriented pure copper monocrystal* is considered. In the following, some conclusions are drawn from the material parameters on the relevance of certain defect populations in the deformation process. Especially, the respective contributions to dynamic recovery through annihilation of screw dislocations after cross-slip and through annihilation of edge dislocations after climb are estimated. On this basis, it can be decided, whether the two dislocation characters have to be treated separately, and whether vacancies have to

Table 1. Effective screw dislocation annihilation length for copper and aluminium at room temperature for different local cell wall dislocation densities.

	Cu	Al
$\gamma_{SF}/J\ m^{-2}$	$55\cdot10^{-3}$	$200\cdot10^{-2}$
$RT/T_m/1$	0.2	0.3
$y_{s,eff}$ ($\rho_w = 10^{14}$ m^{-2} or d_c = 2.4 μm)/b	6	584
$y_{s,eff}$ ($\rho_w = 10^{15}$ m^{-2} or d_c = 0.75 μm)/b	6	831
$y_{s,eff}$ ($\rho_w = 10^{16}$ m^{-2} or d_c = 0.24 μm)/b	36	1591

be taken into account as a relevant defect population.

Materials with intermediate and high stacking fault energies are chosen in order to avoid deformation twinning. Pure metals were used because they do form cells. The annihilation rate of immobile screw dislocations cancelling out after cross slip with mobile screw dislocations of the opposite sign passing by scales with an effective annihilation length $y_{s,eff}$. If the mobile dislocation passes by within this length, an annihilation event takes place (see also subsubsection 3.2.2). Pantleon [61] used the cross-slip model by Escaig [62] – in a version slightly modified for large strains – to calculate the effective annihilation length according to

$$y_{s,eff} = \hat{y}_s \frac{l_{SF}}{b} P_{cs}\left(1+\frac{1}{\chi}\left(e^{-\chi}-1\right)\right)+y_{s,0}. \qquad (4)$$

where the stacking fault width l_{SF} is connected to the stacking fault energy γ_{SF} through

$$l_{SF} = \frac{Gb^2}{16\pi\gamma_{SF}}. \qquad (5)$$

The cross-slip probability P_{cs}, in addition, scales with the cross-slip energy

$$E_{CS} = \frac{Gb^2}{37.3} l_{SF}\sqrt{\ln 2\sqrt{3}\frac{l_{SF}}{b}} \qquad (6)$$

and, especially, with the local shear resistance due to the local dislocation density in the cell walls according to

$$P_{CS} = \exp\left(-\frac{E_{CS}}{k_B T}\left(1+3\frac{\tau b}{\gamma_{SF}}\right)^{-1}\right) = \exp\left(-\frac{E_{CS}}{k_B T}\left(1+48\pi\alpha_w l_{SF}\sqrt{\rho_w}\right)^{-1}\right). \qquad (7)$$

The quantity χ in Eq. (4) expresses a total probability of cross-slip events during penetration of a mobile dislocation through a cell wall, but is irrelevant in the present context because the term in large brackets in Eq. (4) approximately equals 1 for quasistatic deformation of copper as well as aluminium at room temperature. For more details, the reader is referred to [61]. Table 1 displays the effective annihilation lengths for copper and, as a point of reference, also for aluminium at room temperature together with their stacking fault energies [63] and homologous temperatures for three different local cell wall dislocation densities corresponding to three different cell sizes (see below).

One can conclude that – within the framework of the cross-slip model by Pantleon – for cold deformation of copper up to intermediate strains with cell sizes of more than 0.1 μm, the screw dislocation annihilation length for cross-slip is very similar to the edge dislocation annihilation length for dipole disintegration, so that the both characters do not need to be distinguished. For aluminium, on the contrary, the annihilation length of screws is much larger than the one of edges from the beginning of cross-slip, so that one can assume, as a first approximation, that the cell structure consists mainly of edge dislocations. Annihilation of edge dislocations after vacancy-assisted climb can be neglected because low homologous temperatures are considered: bulk diffusion of plastic vacancies is too slow due to the low mobility of the vacancies, and core or pipe diffusion would require significant dislocation densities in the cell interiors (where plastic vacancies are generated by moving jogs in the mobile dislocations) to transport the vacancies to the cell walls (where they would be needed to assist climb and subsequent annihilation of cell wall with mobile dislocations).

2.2. Disclinations

If the formation of fragment boundaries is considered as a *nucleation and growth process*, then it is natural to model fragmentation in terms of *disclina-*

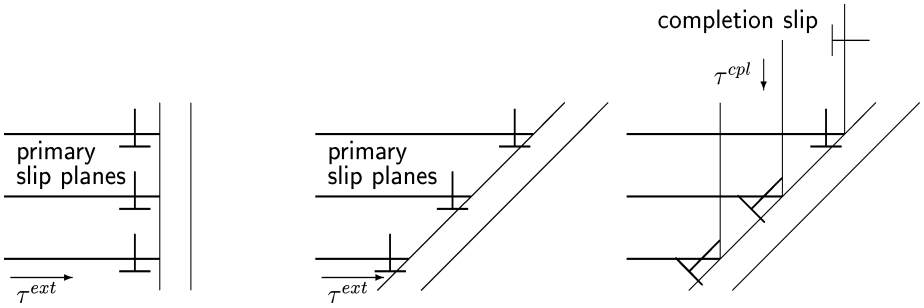

Fig. 4. Left: both-side terminating excess dislocation wall with an ideal LAGB segment structure at an obstacle perpendicular to the primary slip planes. Middle: non-ideal both-side terminating excess dislocation wall with long-range stresses at an obstacle inclined to the primary slip planes. Right: completion slip to complete the non-ideal excess dislocation wall to an ideal LAGB.

tion dynamics. In the present paper, it is assumed that the nucleus of a fragment boundary is a *both-side terminating excess dislocation wall*. Such a wall can be formed by collective stopping of mobile dislocations of the same sign on neighbouring parallel slip planes at an obstacle. If the excess dislocations in the wall are arranged at equal and minimum possible distances, i.e. if they form an *ideal low-angle grain boundary* (LAGB) *segment*, then the *border lines* of the both-side terminating wall are *partial disclinations*. This is, for instance, the case for single slip and an obstacle perpendicular to the slip planes (see Fig. 4, left). If it is not the case, e.g. for single slip and an obstacle inclined to the slip planes (see Fig. 4, middle), the long-range stress fields around the non-ideal dislocation configuration would trigger *Ergänzungsgleitung* [64,65] (completion slip) on additional slip systems to complete the non-ideal both-side terminating excess dislocation wall to an ideal low-angle grain boundary segment (see Fig. 4, right).

Disclinations are the rotational "twin-sisters" of the translational dislocations[1]: *disclinations* are *lines of discontinuity of misorientation*, they separate regions where crystal parts are (already) misoriented with respect to each other from regions where this is not (yet) the case, they *accommodate lattice rotation mismatches*, while *dislocations* are *lines of discontinuity of shear*, they separate regions where crystal parts are (already) sheared with respect to each other from regions where this is not (yet) the case, they *accomodate strain mismatches*. Disclinations were, together with dislocations, introduced into the theory of elasticity by Volterra as early as in 1907 [68]. In a Volterra process, *disclinations* are generated by introducing a cut into an elastically isotropic hollow cylinder, *rotating* the two shores with respect to each other, and inserting the missing or withdrawing the surplus matter. *Dislocations*, on the contrary, are produced by *shifting* the two shores with respect to each other. In a synthetic definition, a *Frank vector* representing *axis* and *angle* of the rotation is introduced in analogy to the *Burgers vector* representing *direction* and *magnitude* of the shift. In an analytic definition, the Frank vector closes the rotation mismatch in a Nabarro circuit [66], as the Burgers vector closes the shift mismatch in a Burgers circuit. Wedge and twist disclination characters are distinguished (Frank vector parallel or perpendicular to the defect line along the cylinder axis, respectively) as edge and screw dislocation characters are distinguished (Burgers vector perpendicular or parallel to the defect line).

However, in contrast to a single dislocation, a single disclination cannot exist in a crystal because of the requirement of coincidence of lattice sites after the Volterra process: after rotating or shifting the two shores of the cut with respect to each other and after inserting the missing or withdrawing the surplus matter, the lattice sites on the two shores of the interfaces have to coincide. In a crystal, this requirement can only be fulfilled for angles of at least 60 degrees which would obviously cause fracture. It was only in the early 1970s that scientists in the USA [67,69,70] started to consider *dipoles of partial disclinations* and researchers in Russia proposed *networks* [16,20] and other *self-screening configurations* [71] of partial disclinations rather than single perfect disclinations. Such partial disclination dipoles as new entities can fulfill the crystallographic requirements because the two rotations compen-

[1] For introductory texts on disclinations see, for instance, [23,66,67].

sate mutually at large distances from the dipole and leave only a net shift behind, comparable to a "superdis-location" [23]. Therefore, the dipole configuration allows the realization of partial disclinations with low strenghts $+\omega$ and $-\omega$ in a crystal. Note that it thus also allows the *free variation*[1] of the magnitude of the mutually compensating rotation angles or disclination strengths $+\omega$ and $-\omega$, and it introduces the dipole width $2a$ as an additional variable. While *dislocation modelling* works with only *one* variable, namely the *dislocation density*, *disclination modelling* has to deal with *three*, namely the *disclination dipole density* and the average *disclination strengths* and *dipole widths*.

A *partial disclination* with a low strength ω can then be *"translated"* into the *border line of a terminating low-angle grain boundary* with misorientation $\varphi = \omega$ in the sense that both representations exhibit the same long-range stress field. More specific, a partial wedge disclination can be "translated" into the border line of a terminating regular excess edge dislocation wall (see Fig. 5), and a partial twist disclination can be "translated" into the border line of a terminating regular screw dislocation net.

However, these "translations" are *non-unique*: a partial wedge disclination dipole can, for instance, be "translated" into a both-side terminating excess dislocation wall of only one sign as well as into two parallel semi-infinite excess dislocation walls of opposite signs (see Fig. 6). Both of these configurations exhibit the same long-range stress field.

In this way, in principle all partial disclination configurations in a crystal can be "translated" into, possibly complex, dislocation configurations[2] . The advantages of a disclination description are its mathematical simplicity and its correspondence with certain ideas of large-strain plastic deformation and work-hardening: if fragmentation is considered as the essential feature of large-strain plastic deformation and is understood as a process of nucleation and growth of fragment boundary segments, i.e. as an activation of rotational modes of deformation

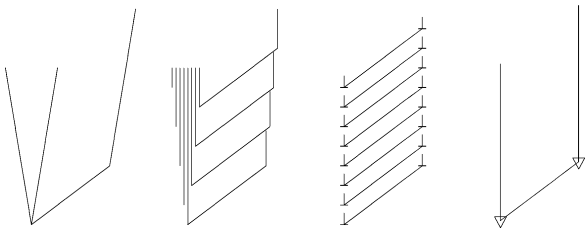

Fig. 5. "Translation" of a partial wedge disclination into the "language" of dislocations: (a) wedge of matter to be inserted in the Volterra process, (b) package of semi-infinite crystallographic planes with equidistant border lines, (c) semi-infinite wall of parallel excess edge dislocations with equal and minimum possible distances, (d) partial wedge disclination.

through cooperative motion of dislocations, then these ideas can be implanted in a plastic deformation model by describing fragmentation in terms of generation of partial disclination dipoles and propagation of partial disclinations through capturing of mobile dislocations. If large-strain work-hardening is supposed to be due to long-range stresses and if these long-range stresses are assumed to be *Randspannungen* (border stresses) around the border lines of fragment boundary segments with a for the rest ideal low-angle grain boundary structure, then the long-range stress fields can properly be expressed as partial disclination stress fields. In fact, the situation is similar with dislocations: In principle, all dislocation configurations can be "translated" into, possibly complex, atom configurations. The advantages of the dislocation description are again its mathematical simplicity and, above all, its correspondence with the idea and experimental evidence that plastic deformation is carried out by progressive slip on glide planes, i.e. by the activation of translational modes of deformation through collective motion of atoms. Therefore, it is improper to consider disclinations as a mere modelling tool introduced only for mathematical convenience. Representing a complex configuration of many dislocations, disclinations are probably just as much physical objects as dislocations, representing a complex configuration of many atoms, are. The key experimental task is to confirm (or reject) that dislocations are indeed arranged in configurations corresponding to partial disclinations and that long-range stresses indeed exhibit the functional decay typical for partial disclinations (see below).

The consideration of partial disclination dipoles was the first keystone to the introduction of

[1] If the partial disclination with strengths ω represents the tip of a terminating low-angle grain boundary with misorientation φ (see below), the allowed strength is discretized in multiples of $\Delta\varphi = b/h^{min}$ where h^{min} is the minimum dislocation spacing in a low-angle grain boundary. This discretization is so fine that it can be neglected in the present considerations.

[2] This does, of course, not hold for non-crystalline materials where disclinations can directly act as carriers of plastic deformation.

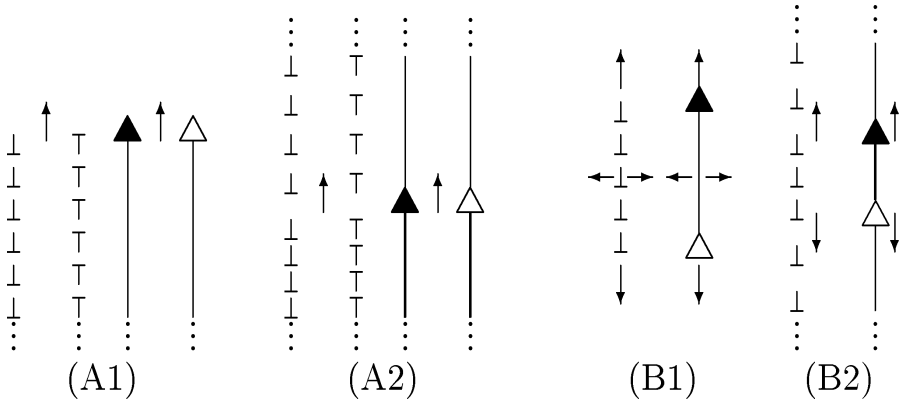

Fig. 6. Partial disclination dipoles of the four configurations considered above. On the left in the language of dislocations, on the right in the language of disclinations.

disclinations into crystal plasticity because it became clear that (partial) disclinations could exist in real crystals. The "translation" of partial dislocation dipoles into dislocation configurations was the second one because it opened the door to coupling dislocation and disclination dynamics and actually establishing disclination dynamics in real crystals.

Motivated by TEM micrographs showing pairs of parallel terminating fragment boundaries with opposite misorientations (see e.g. [10,18,72], cf. the scheme (A1) in Fig. 6), Romanov and Vladimirov [22,23] were the first to model the *growth of a misorientation band* in terms of the *propagation of a partial wedge disclination dipole* at the top of the band. The partial disclination dipole was proposed to propagate by widening dislocation loops ahead of the dipole with the help of its long-range stress field, capturing the edge components, attaching them to the backward terminating boundaries, thereby shifting the border lines of the terminating boundaries and propagating itself. Similarly, a both-side terminating excess dislocation wall, can as already discussed by Nabarro [73] and Li [74] in the context of polygonization, act as a "nucleus" of a fragment boundary, expand or "grow" by *capturing additional mobile dislocations* through the long-range stress fields around its tips, and thus "polygonize" the matrix. A propagating partial disclination, in contrast to a perfect one, thus leaves a *track* behind, namely a *fragment boundary*, like a gliding *partial dislocation*, in contrast to a perfect one, leaves a *stacking fault* behind.

If, finally, such a propagating partial disclination gets stopped at an existing fragment boundary, a rotation mismatch should be left behind around the new triple junction (see Fig.7). Formally, this mismatch could be detected by carrying out a Nabarro circuit [66] around the triple junction. A rotation mismatch around the triple junction would then correspond to an immobile partial disclination in the node line.

Experimental evidence for such a rotation mismatch around fragment boundary triple junctions and thus for the presence of partial disclinations

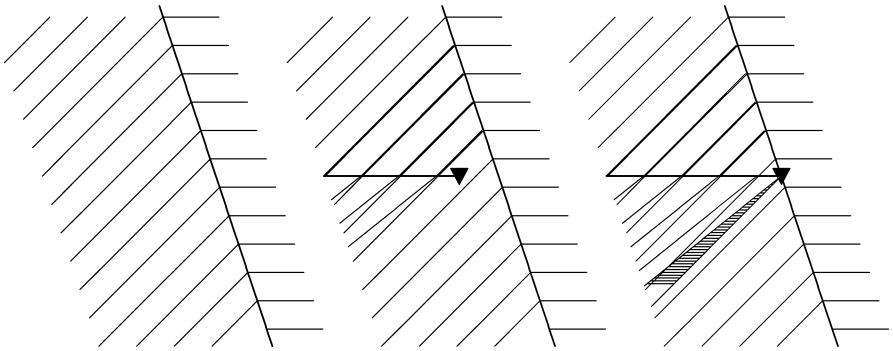

Fig. 7. Formation of a new fragment boundary triple junction through a partial disclination propagating at the top of an arising fragment boundary and getting locked in an existing one. The new triple junction carries an orientational mismatch and is thus a noncompensated node.

was recently found by Klemm and coworkers [75,76] in TEM microdiffraction measurements at cold-rolled copper mono- and polycrystals. The misorientations across the three joining fragment boundaries were determined and the product of the misorientation matrices was found to deviate from the identity. In the linear approximation, the sum of the misorientation vectors was found to deviate from zero. Furthermore, when shifting the electron beam along the joining boundaries, the local orientation was found to vary continuously.

Further methods were used to demonstrate the presence of partial disclinations in the substructure of deformed metals: Koneva, Kozlov and coworkers [38-42] used TEM bending contour measurements to analyse the magnitude and the functional decay of the long-range stress fields around terminating subboundaries and found them to match with the ones of the partial disclination stress fields. Tyumentsev et al. [77] used TEM reflex width measurements to determine lattice bend-twist tensor components along grain boundaries in ultra-fine grained copper and nickel crystals produced through severe plastic deformation. The measured variation of the bend-twist tensor components along matched with the one to be expected for a pile-up of partial disclinations on the grain boundary. Recently, the present author proposed to use scanning tunnel microscopy (STM) to study the surface etching around the points where fragment boundary triple junctions leave to the surface. Preferred etching might indicate that the nodes are non-compensated and include partial disclinations [78].

2.3. Reaction kinetics

The evolution of a global average defect density with time or strain is determined by the elementary mechanisms of generation and annihilation of the defects and of reactions of defects in the population under consideration with defects in other populations. These elementary mechanisms depend on the material and process parameters. Therefore, a rate equation which describes the time or strain evolution of a, say, global dislocation density ρ_i, has the formal structure

$$\frac{d\rho_i}{dt} = F(c_1,\ldots,c_k,\rho_1,\ldots,\rho_i,\ldots,\rho_l, S_1,\ldots,S_m,m_1,\ldots,m_n,p_1,\ldots,p_o), \tag{8}$$

where the c's denote point defect concentrations, the ρ's and S's line and plane defect densities and the m's and p's material and process parameters, respectively. The earliest representant of this class of evolution equations was Gilman's equation [79] for a dislocation density undergoing multiplication and pairwise annihilation. Another commonly used example, proposed for the shear strain γ instead of the time as an evolution parameter, is Kocks' semi-phenomenological equation [80]

$$\frac{d\rho}{d\gamma} = \frac{1}{\beta b}\sqrt{\rho} - \frac{L_a}{b}\rho \tag{9}$$

for a forest dislocation density ρ with storage and dynamic recovery. For single slip or symmetric multiple slip, the strain increment can be expressed in terms of the shear strain increment, $d\varepsilon = m_S n\, d\gamma$, giving Kocks' and Mecking's law [81]

$$\frac{d\rho}{d\varepsilon} = k_1\sqrt{\rho} - k_2\rho. \tag{10}$$

However, at intermediate and large strains, dislocation patterning takes place, so that a representation of the dislocation structure in terms of one global dislocation density becomes improper. Two routes were followed to tackle this problem: On one of them, the global defect densities were replaced by local ones and the evolutions of the local defect densities were considered not only as a time-, but as a time- and space-dependent problem. The evolution equations then have the structure of continuity equations,

$$\frac{d\rho_i}{dt} = F(c_1,\ldots,c_k,\rho_1,\ldots,\rho_i,\ldots,\rho_l, S_1,\ldots,S_m,m_1,\ldots,m_n,p_1,\ldots,p_o) - \nabla \boldsymbol{j}_i \tag{11}$$

Orlov [82] proposed already in 1965 to consider the dislocation density separately for the slip systems. According to Malygin [83], one obtains a system of partial differential rate equations with the structure

$$\frac{\partial\rho^{(i)}}{\partial t} + \nabla\left(\overline{v^{(i)}}\rho^{(i)}\right) = n^{(i)}\overline{v^{(i)}} + \sum_p \frac{\overline{v^{(i)}}}{l_p^{(i)}}\rho^{(i)}. \tag{12}$$

While Malygin's models are restricted on a consistent description of the first three stages of plastic deformation, including smooth transitions between these three stages, the present paper aims at an extension of the models to the later stages of plastic deformation, that is to large strain plastic deformation, by transferring the framework proposed by Malygin for dislocation kinetics to disclination kinetics,

$$\frac{\partial \theta^{(w)}}{\partial t} + \nabla\left(\overline{V^{(w)}}\theta^{(w)}\right) = n^{(w)}\overline{V^{(w)}} + \sum_p \frac{\overline{V}^{(w)}}{l_p^{(w)}}\theta^{(w)}. \quad (13)$$

On the second route, the transport terms were neglected, and a substructure geometry was *imposed* instead by implementing phenomenological scaling laws like a principle of similitude (see below) into the model. As far as patterning is concerned, the present paper follows this second route.

2.4. Plastic deformation and work-hardening

Following Kocks, Argon and Ashby [84], the local effective shear stress[1] is defined as[2]

$$\hat{\tau}_{ij}^{eff} = \hat{\tau}_{ij}^{ext} - \hat{\tau}_{ij}^{int}, \quad (14)$$

where the internal shear stress $\hat{\tau}_{ij}^{int}$ is by definition taken positive in the direction opposing the applied external shear stress $\hat{\tau}_{ij}^{ext}$. The local effective shear *stress* $\hat{\tau}_{ij}^{eff}$ would then be opposed by the local shear *resistance*[3] $\hat{\tau}_{ij}^{*}$ so that the material would (plastically) shear, if

$$\left(\hat{\tau}_{ij}^{ext} - \hat{\tau}_{ij}^{int}\right) - \hat{\tau}_{ij}^{*} = \hat{\tau}_{ij}^{eff} - \hat{\tau}_{ij}^{*} \geq 0 \quad (15)$$

would hold. In case of *athermal* deformation, the equality applies.

The local shear resistance of a crystalline metal is governed by glide obstacles as solute atom concentrations, local dislocation densities, twin, grain or phase boundaries and/or, in the sense of an organized shear resistance [58], by long-range stress fields of static or dynamic origin, in as far as these stress fields do not directly act as back stresses in the active slip systems. Since the present paper discusses only pure metals with intermediate and high stacking fault energies, the following considerations are restricted to local shear resistances due to local dislocation densities and long-range stress fields. The local dislocation density contributes to the local shear resistance through the elastic and contact interaction between intersecting dislocations, as described, for instance, in the Hirsch-Saada process [85,86]. The long-range stress fields can hinder the dislocation motion in two different ways: either directly by reducing the local effective stress through the components acting as back stresses on the slip planes [87], or indirectly through an organized shear resistance connected to the locally stored elastic strain energy due to the components not acting as back stresses [58].

Long-range stresses can be explained from two different points of view: From the *defect theory* or *static* point of view, *high-energy dislocation arrays*, like pile-ups or terminating excess dislocation walls (with *Randspannungen* (border stresses) around their borders, cf. [60]), cause long-range stresses. Such dislocation configurations evolve from dislocation dynamics and reflect the deformation history on the defect level. However, the evolution of dislocation configurations exhibiting long-range stresses is limited by the micromechanical compatibility requirements (see below). From the *micromecha-nics* or *dynamic* point of view, *elastic strain mismatches* cause long-range stresses. Such mismatches result from compatible deformation of plastically heterogeneous materials and reflect the deformation history on the stress and resistance level [48]. For example, at intermediate strains, *dislocation patterning* leads to spatially varying local shear resistances. Applying an external load to such a "compound" material (made up of a "soft phase" with low dislocation density ρ_c and shear resistance τ_c^* and a "hard phase" with high dislocation density ρ_w and shear resistance τ_w^*) gives *elastic* strain mismatches and thus elastic misfit stresses [48]. The corresponding *plastic* strain mismatches can, following Nye and Kröner [88,89], be "translated" into densities of *misfit dislocations* (also called "geometrically necessary dislocations" [90]). However, these densities do not provide any information on the spatial distribution, on the configuration of the misfit dislocations and thus also not about possible long-range stress fields due to the configuration. In an ideal case, a misfit dislocation configuration can be found which exhibits a long-range stress field that equals the elastic misfit stress field and dislocation dynamics can be used to study how this configuration arose in the course of plastic deformation. However, in other cases it is impossible to find such a configuration because the calculated "virtual" misfit dislocations are non-crystallographic [58].

In any case, local elastic misfit stresses $\Delta\tau_c^{mis}$ and $\Delta\tau_w^{mis}$ due to different local shear resistances in different "phases" are self-equilibrated *local internal stresses*. In the *global* average over the specimen, they, weighted with the respective volume fractions $(1-\xi)$ and ξ of the "phases", have to sum up to zero,

[1] The microscopic resolved shear stresses and shear strains are denoted as τ and γ; the macroscopic stresses and strains are denoted as σ and ε.

[2] Tensorial quantities are marked with $\hat{a}$.

[3] The resistances are marked with an asterisk * in order to distinguish them from the stresses.

$$(1-\xi)\Delta\tau_c^{mis} + \xi\Delta\tau_w^{mis} = 0. \qquad (16).$$

Therefore, they can contribute to the *local effective stress* and/or to the *local shear resistance* but do not *directly* affect the *global* flow stress. If, however, their contribution to the local shear resistance, in the sense of an organized shear resistance [58], is significant compared to the one of the local dislocation density, then the elastic misfit stresses *do* affect the global flow stress.

If one considers, following Argon and Haasen [58] or Pantleon and Klimanek [61,91], a "compound" made up of a cell wall "phase" with high dislocation density and a cell interior "phase" approximately void of dislocations, then the local shear resistance in the cell interior "phase" is entirely controlled by the long-range elastic misfit stresses. In the following, two simplified examples are discussed in more detail. During uniaxial deformation of copper single crystals with a high-symmetric orientation, multiple slip is activated and a cell structure with cell walls parallel and perpendicular to the load axis is formed [55]. The elastic strain mismatches arising due to the different local shear resistances cause internal misfit stresses. The corresponding plastic strain mismatches can be "translated" into regular layers of misfit dislocations at the interfaces between cell walls and cell interiors. As long as the local shear resistance in the cell walls increases faster than the one in the cell interiors, the plastic strain mismatch increases and misfit dislocations are accumulated at the interfaces according to [61]

$$N_{mis} = \frac{1-\nu}{2}\frac{\tau_w^* - \tau_c^*}{Gb_{res}m_S}, \qquad (17)$$

where N_{mis} and b_{res} denote the line density and the resultant Burgers vector of the misfit dislocations and m_S is the Schmid factor. In this example, the regular layers exhibit long-range stress fields corresponding to the elastic misfit stresses. These long-range stress fields *assist* the applied stress in the cell *walls* and *counteract* it in the cell *interiors*. They have strong components which act as back stresses and reduce the local effective stress in the cell interiors and only weak components which do not act as back stresses but might produce an organized shear resistance and raise the local shear resistance that the local effective stress stress has to overcome in the cell walls. However, a detailed consideration by Pantleon (appendix D in [61]) showed that an estimation of the flow stress taking the long-range stress fields into account differs only by 3% from an estimation ascribing the compound deformation resistance fully to the local dislocation density in the cell walls or to the smeared-out global dislocation density. Therefore, the present paper neglects the long-range stresses due to misfit dislocation configurations.

One can conclude that there are two "damping" or "inhibiting" mechanisms limiting the growth of elastic and plastic strain gradients or the accumulation of misfit dislocations: One of them is dynamic recovery which counteracts and finally balances dislocation storage in the cell walls, and the other is the generation of internal misfit stresses. In this way, the difference between the two local shear resistances is restricted. This is required for stable plastic deformation [92] because misfit stresses associated with elastic strain gradients scale with the (huge) shear modulus *G* according to

$$(\sigma_w - \sigma_c) = -\alpha G(\varepsilon_w - \varepsilon_c). \qquad (18)$$

In the case of single slip with cell walls perpendicular to the slip direction, the situation is more difficult. Again, elastic strain mismatches and misfit stresses arise, but if one would "translate" the corresponding plastic strain mismatches into regular layers of misfit dislocations at the interfaces, these layers would not exhibit any long-range stress fields because they would represent ideal low-angle grain boundary (LAGB) configurations. This problem could be overcome by, for instance, considering the two single layers to the both sides of a (narrow) cell wall together as a double layer which does not have long-range stresses *outside* the double layer (i.e. in the cell interiors in this case), but *inside* (i.e. in the cell walls). Gil Sevillano and Torrealda [93,94] proposed that the long-range stresses inside the layer would result in the activation of additional slip systems to ensure homogeneous deformation, so that the cell walls would rotate with respect to the cell interiors. Straight long excess dislocations stopping at the interface would then serve to accommodate *lattice rotation mismatches* rather than *strain mismatches*. Another way to overcome the problem would be to consider layers with irregular excess dislocation distributions which do exhibit long-range stresses [95,96]. The latter approach would result in locally varying misorientations across the layers, i.e. between cell walls and cell interiors, and, in general, also to finite *locally varying net misorientations* across the double layers, i.e. between neighbouring cells.

The present paper follows the latter approach in a more "schematic" way (for details, see below). The excess dislocations are assumed to be arranged

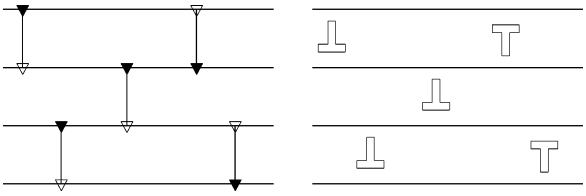

Fig. 8. Left: a brick-shaped fragment structure with the immobilized partials of partial disclination dipoles in the fragment boundary triple junctions. Right: a pile-up configuration with the same long-range stress field.

.

in *layer segments* with a *regular* dislocation distribution, so that the misorientation varies only around the border lines of the segments. These layer segments are considered as a result of incidental collective stopping of neighbouring straight long excess dislocations at the interfaces. If a layer segment has an *ideal low-angle grain boundary (LAGB) configuration*, it corresponds to a *dipole of partial disclinations* at the borders lines of the group.

In the early stages I and II of plastic deformation, the spacing between the excess dislocations in the layer segments would remain large, so that the misorientation across the layer segment and the end stresses around its border lines would remain too small to capture additional mobile dislocations and thus too small to let the layer segment expand. Consequently, short excess dislocation layer segments would cover the cell wall on both sides in a more or less irregular way, with locally varying, but largely mutually balancing misorientations (see Fig. in subsection 3.2.3.). However, in stage III of plastic deformation, the misorientation across the layer segments and the end stresses around its border lines would get *sufficiently large to capture additional mobile dislocations and to expand along the cell wall* (see Fig. in subsection 3.2.4.). If such a layer segment is *not balanced* by its counterpart on the other side of the cell wall, it causes local *net misorientations* across the cell wall and spreads this net misorientation out over the whole cell wall. In this way, it acts as a *nucleus* of a fragment boundary layer which *grows* along the cell wall. If a layer segment has an ideal LAGB configuration, its growth corresponds to the *propagation* of the two partial disclinations along the cell wall.

In this picture, the build-up of strain mismatches at the interfaces between cell walls and cell interiors is restricted by the transition from balanced to non-balanced stopping of straight long excess dislocations. The stopped excess dislocations then serve to accommodate *lattice rotation* rather than *strain mismatches*. The transition from *translational* to *rotational* modes of deformation is thus *required by micromechanics*, namely to inhibit further build-up of strain mismatches, and is *realized by dislocation dynamics* through switching from balanced to non-balanced stopping, essentially due to a reduction of the spacing between the stopped excess dislocations as a result of bundling mobile dislocations in slip bands (for details, see below). If one assumes an ideal LAGB configuration of the layer segments, the transition from translational to rotational modes of deformation corresponds to the transition from *dislocations gliding individually along slip planes* to *disclinations propagating along cell walls* (which is, of course, realized by dislocations gliding collectively along slip planes).

In the proposed picture, the more or less irregular distribution of (strain) misfit dislocation layer segments on both side of the obstacle in the early stages I and II exhibits long-range stresses – not through the layers itself, but through their ends – which resemble the elastic misfit stresses. These long-range stress fields are required by micromechanics, form a self-equilibrated set and do not contribute to the global flow stress. The expanding (lattice rotation) misfit dislocation layers on one side of the cell wall in the late stages III and IV also exhibit long-range stresses – again not through the layers themselves, but through their ends. However, these long-range stress fields are a consequence of the nucleation and growth mechanism of fragment boundary layer formation, are connected to the propagating partial disclinations as carriers of the rotational modes of deformation, do not form a self-equilibrated set and do contribute to the global flow stress. The partial disclination dipoles (PDDs) have the same pleasing feature as traditional pile-ups that their long-range stress fields affect the local effective stress by acting as back stresses on mobile dislocations on the primary slip plane.

Consequently, the global flow stress resulting from the substructure is calculated from two contributions:

- the local shear resistances τ_w^* and τ_c^* of the cell walls and cell interiors, respectively,
- the long-range internal back stresses τ_ω^{int} due to the partial disclination dipoles (PDDs).

According to Eq.(15), the local effective stress has to overcome the local shear resistances τ^*,

$$\tau^{eff} = \tau^{ext} - \tau^{int} \geq \tau^* . \qquad (19)$$

In the present paper, only the contributions of the local dislocation densities to the *local shear*

resistances in the cell walls and cell interiors are taken into account. The contributions of long-range stress fields due to misfit dislocation configurations accommodating plastic *strain* mismatches, in the sense of organized shear resistances, are neglected. Furthermore, the local dislocation density ρ_c in the cell interiors is considered to be negligible compared to the one ρ_w in the cell walls, so that the compound shear resistance is entirely controlled by the local dislocation density in the cell walls. Therefore, one ends up with

$$\tau_c^* = \alpha G b\sqrt{\rho_c} << \tau_w^* = \alpha G b\sqrt{\rho_w} \tag{20}$$

for the local shear resistances and with ($\overline{\rho_w}$ – smeared-out global dislocation density)

$$\tau^* = \xi\tau_w^* + (1-\xi)\tau_c^* \approx \xi\tau_w^* = \xi\alpha G b\sqrt{\frac{\overline{\rho_w}}{\xi}} = \sqrt{\xi}\alpha G b\sqrt{\overline{\rho_w}} \tag{21}$$

for the compound shear resistance.

Correspondingly, the *local internal stresses* are proposed to be entirely controlled by the long-range stress fields due to partial disclination dipoles which correspond to both-side terminating excess dislocation layers accomodating plastic *lattice rotation* mismatches. Long-range stress fields due to misfit dislocation configurations accommodating plastic *strain* mismatches, are again neglected. In the case of single slip, irregular distributions of excess dislocation layer segments on both sides of the cell walls would cause back stresses, but, according to Saada [95,96], those would remain small compared to the stress fields due to PDDs. In the case of multiple slip, regular distributions of misfit dislocations from the symmetrically active slip systems would generate back stresses, but, according to Pantleon [61], taking into account these effects would only slightly change an estimation of the flow stress. Since the "wavelength" of the fragment structure is large compared to the one of the cell structure (or the mean distance between the partial disclinations is large compared to the one between the dislocation cell walls), and since, in the case of single slip, the dipole arm is perpendicular to the slip plane, a global average internal back stress $\overline{\tau_\omega^{int}}$ is considered. The long-range stress field of such PDDs with disclination strength ω and dipole arm $2a$ are the same as the ones of pile ups with a "super Burgers vector" $B = \omega a$, so that an internal back stress arises,

$$\overline{\tau_\omega^{int}} = \alpha G B\sqrt{2\theta_{tot}} = \alpha G\omega a\sqrt{2\theta_{tot}} = \alpha G\omega a\sqrt{\theta_p + 2\theta_i} \approx \alpha G\omega a\sqrt{2\theta_i}, \tag{22}$$

where θ_p denotes the density of PDDs with propagating partials and θ_i and θ_{tot} denote the immobile and total partial disclination density, respectively[1]. If the fragment structure arises from generation and expansion of PDDs and immobilization of their partials and consists of fragment boundaries with ideal LAGB configurations and non-compensated triple junctions with partial disclinations (see Fig. 8), then the average fragment boundary spacing d_f corresponds to the dipole width $2a_i$ between the immobilized partials of the PDDs.

With

$$2a_i \approx d_f = \frac{K_f}{\sqrt{\theta_i}}, \tag{23}$$

where K_f is a geometry factor depending on the assumed mosaic geometry of the fragment structure (see below), one finds

$$\overline{\tau_\omega^{int}} \approx \frac{1}{\sqrt{2}}\alpha G K_f\omega. \tag{24}$$

Assuming the disclination interaction coefficient β to be $\beta = \alpha K_f / \sqrt{2}m_s$, this matches with the flow stress contribution

$$\Delta\sigma_\omega = \beta G\omega \tag{25}$$

proposed by Romanov and Vladimirov [23]. Distributing the available excess dislocation density ρ_{exc} on the total surface per unit volume of the fragment boundary layers "drawn" by the propagating partial disclinations gives the misorientation

$$\varphi \approx \frac{b}{h} = bN_{exc} = f_f^{geom}\frac{b\rho_{exc}}{\sqrt{\theta_i}}, \tag{26}$$

where f_f^{geom} is another geometry factor depending on the assumed mosaic geometry of the fragment structure (see below). It is now assumed that the immobile partial disclination strength ω, i.e. the mean orientation mismatch around a non-compensated triple junction, is equal to the current mean misorientation φ. In a simplistic picture for a triple junction formed by the two halfs of an "old" fragment boundary and a "new" boundary, all with the same

[1] Note that θ_p thus is a disclination *dipole* density, while θ_i and θ_{tot} are *single* disclination densities.

mean misorientation, this makes sense because the misorientations across the two halfs of the "old" boundary compensate each other, so that the net orientation mismatch is equal to the misorientation across the "new" boundary. Finally, one ends up with

$$\overline{\tau_{\omega}^{int}} \approx \frac{1}{\sqrt{2}}\alpha G K_f \varphi = \frac{1}{\sqrt{2}}\alpha G b K_f f_f^{geom} \frac{\rho_{exc}}{\sqrt{\theta_i}}. \quad (27)$$

The flow stress to be applied for athermal plastic deformation thus is

$$\sigma_f = \frac{1}{m_S}\left(\tau^* + \overline{\tau_{\omega}^{int}}\right) = \frac{1}{m_S}\left(\sqrt{\xi}\alpha G b\sqrt{\overline{\rho_w}} + \frac{1}{\sqrt{2}}\alpha G K_f \varphi\right) = \frac{1}{m_S}\left(\sqrt{\xi}\alpha G b\sqrt{\overline{\rho_w}} + \frac{1}{\sqrt{2}}\alpha G b K_f f_f^{geom}\frac{\rho_{exc}}{\sqrt{\theta_i}}\right). \quad (28)$$

This corresponds with the phenomenological laws proposed by Gil Sevillano, Van Houtte and Aernoudt [97],

$$\Delta\sigma \propto \frac{\sqrt{\varphi}}{\sqrt{d_f}} \quad \text{with} \quad \varphi \propto \frac{1}{d_f}, \quad (29)$$

and by Kozlov and Koneva [42],

$$\Delta\sigma \propto \varphi. \quad (30)$$

3. A WORK-HARDENING MODEL FOR STABLE ORIENTATIONS

3.1. Schematization of the substructure

The work-hardening model to be discussed in this section is designed for a single crystal with a stable symmetric orientation, i.e. for a constant Schmid factor m_S and for multiple slip right from the beginning of plastic deformation. A cell structure is then formed soon. Therefore, the model starts from a well-developed cell structure consisting of a cell wall "phase" with a high *local* dislocation density ρ_w and a high shear resistance τ_W^* and a cell interior "phase" with a low *local* dislocation density ρ_c and a low shear resistance τ_c^* [48,53].

As mentioned in subsection 2.4, most of the work-hardening models for intermediate and large strains are based on such a two-"phase" compound representation of a cell structure and ascribe the shear resistance of the cell interior "phase" to a local dislocation density. Argon and Haasen [58] and Pantleon and Klimanek [61], on the contrary, referred to abundant TEM evidence – on the unloaded as well as on the neutron-pinned loaded state – for an only negligibly small dislocation density in the cell interior and ascribed the shear resistance of the cell interior "phase" to long-range stresses. The present work follows the latter reasoning and considers the local dislocation density in the cell interiors to be negligible compared to the one in the cell walls,

$$\rho_c << \rho_w = \frac{\overline{\rho_{tot}}}{\xi}, \quad (31)$$

so that the total (*global* average) dislocation density $\overline{\rho_{tot}}$ is obtained by "smearing out" the wall dislocation density from the wall volume fraction ξ to the whole volume.

It is assumed that the mean cell size d_c and the total ("smeared-out") dislocation density $\overline{\rho_{tot}}$ are connected by a Holt-type scaling law [98,99],

$$d_c = \frac{K}{\sqrt{\overline{\rho_{tot}}}} = \frac{K}{\sqrt{\xi\rho_w}}, \quad [32]$$

where K denotes a material constant (cf. e.g. the review paper by Raj and Pharr [100]). Furthermore, it is assumed that a principle of similitude holds throughout the whole course of plastic deformation, i.e. that the volume fraction ξ of the cell wall "phase" remains constant,

$$\xi = f_{geom}\frac{w}{d_c}, \quad (33)$$

where f_{geom}= 2 is a geometrical factor reflecting the elongated shape of the cells and w denotes the cell wall width.

From the elementary processes of fragment boundary nucleation and growth as discussed below in subsections 3.2.3 and 3.2.4, it follows that fragment boundaries evolve as excess dislocation layers along existing cell walls. These excess dislocation layers accomodate the lattice rotation mismatch and in this sense resemble Ashby's "geometrically necessary dislocations" or Mughrabi's "interface dislocations" accomodating either a strain or a lattice rotation mismatch. They are arranged in low-angle grain boundary (LAGB) configurations, so

that the misorientation φ can be calculated from the dislocation spacing h in the wall via the Read-Shockley law which in the case of a single-component LAGB (i.e. an LAGB made up of excess dislocations from only one slip system) reads

$$\varphi \approx \frac{b}{h}. \tag{34}$$

The dislocation spacing h or the excess dislocation line density per area on the fragment boundaries can be derived by distributing the (smeared-out) excess dislocation volume density $\overline{\rho_{exc}}$ on the available total fragment boundary surface S. In order to calculate the latter, one has to make an assumption on the geometry of the fragment structure. While during the early stages of fragmentation, a Poisson-Voronoi mosaic geometry seems to be appropriate (i.e. a random distribution of nucleation points is generated and each place in space is then assigned to the closest of these nucleation points, cf. e.g. [101,102], – a principle which is known from the Wigner-Seitz cells in Solid State Physics), in the developed or later stages a simple parallelepipedal mosaic with "brick-shaped" fragments seems to reflect reality better [58,103]. In this paper, the first will be applied.

In a Poisson-Voronoi mosaic, the mean node line length per unit volume corresponds to the mean triple junction line length per unit volume in a fragment boundary mosaic, i.e. to the immobile partial disclination density θ_i. The mean chord length of the Poisson-Voronoi cells corresponds to the mean chord length of the fragments which is a good measure for the mean fragment size d_f [102]. The mean surface area of the Poisson-Voronoi cells, finally, corresponds to the mean fragment boundary area S_{fb} per unit volume in a fragment boundary mosaic. All three quantities can be expressed through the density of nucleation points of the Poisson-Voronoi mosaic (for details, see [101,102]), so that all three quantities can also be expressed through each other,

$$d_f \approx \frac{166}{\sqrt{\theta_i}}, \tag{35}$$

$$S_{fb} \approx 121\sqrt{\theta_i}. \tag{36}$$

Distributing the available (smeared-out) excess dislocation density $\overline{\rho_{exc}}$ on the total fragment boundary surface area S_{fb} per unit volume then gives the mean excess dislocation spacing in the fragment boundary or, using the Read-Shockley formula Eq. (34), the mean misorientation across the fragment boundaries,

$$\varphi \approx b\frac{\overline{\rho_{exc}}}{121\sqrt{\theta_i}}. \tag{37}$$

The dislocation substructure is thus charac-terized in terms of the following dislocation densities:

– the (smeared-out) redundant cell wall dislocation density ρ_w,
– the (smeared-out) non-redundant excess dislocation density $\underline{\rho_{exc}}$ in the fragment boundary layers,
– the density of dipoles of propagating partial disclinations θ_p at the border lines of the excess dislocation layers
– the density of immobile partial disclinations θ_i in the fragment boundary triple junctions.

3.2. Elementary processes

3.2.1. Dislocation storage: trapping of mobile dislocations into cell walls. Mobile dislocations get stored in the material by trapping into cell walls. Slip line measurements by Ambrosi and Schwink [104] indicated that the mean free path of mobile dislocations is about three times larger than the mean cell size d_c and thus revealed that cell walls are semi-transparent obstacles. A fraction of $P_c \approx 1/3$ of the arriving mobile dislocations gets trapped in the cell wall, while the remaining fraction of about 2/3 penetrates through the wall. (The point of view that all arriving mobile dislocations get trapped at the one side of the wall and in 2/3 of all trapping events another dislocation gets remobilized and emitted at the other side, is formally equivalent to the reasoning suggested above.) For single slip, this results in a storage rate for the *local* cell wall dislocation density of [61]

$$\left(\frac{d\rho_w}{dt}\right)^{+} = \frac{P_c}{w}\bar{v}\rho_m = \frac{P_c}{w}\frac{\dot{\gamma}}{b}, \tag{38}$$

or, for multiple slip on n symmetrically activated slip systems,

$$\left(\frac{d\rho_w}{dt}\right)^{+} = \frac{P_c}{w}n\bar{v}\rho_m = \frac{P_c}{w}n\frac{\dot{\gamma}}{b}, \tag{39}$$

where $\bar{v}$ is the average dislocation velocity, w the cell wall width, and $\dot{\gamma}$ denotes the shear strain rate. Using the principle of similitude (33) and the Holt-type scaling law (32), this can be transformed into the well-known Kocks storage term (cf. eq. (9)), now for a smeared-out cell wall dislocation density,

$$\left(\frac{d\bar{\rho}_w}{dt}\right)^{+} = -\left(\frac{d\rho_m}{dt}\right)^{-} = -\frac{P_c f_{geom}}{d_c} n \frac{\dot{\gamma}}{b} = -\frac{P_c f_{geom}}{K} \sqrt{\bar{\rho}_w}\, n \frac{\dot{\gamma}}{b}. \quad (40)$$

3.2.2. Dislocation dynamic recovery: annihilation of mobile with cell wall dislocations. Stored cell wall dislocations can, on the other hand, annihilate with mobile dislocations of opposite sign passing by. In the case of edge dislocations, such annihilation events can take place through dipole disintegration, as proposed by Essmann and Mughrabi [105], or after vacancy-assisted climb. In the case of screw dislocations, annihilation events take place after cross-slip. As discussed in subsection 2.1, room temperature deformation of copper is characterized by comparable annihilation lengths y_s of screws after cross-slip and y_e of edges after dipole disintegration. Annihilation of edges after vacancy-assisted climb can be neglected because bulk diffusion of plastic vacancies is too slow at low homologous temperatures, while core or pipe diffusion would require a significant dislocation density in the cell interior (where the plastic vacancies would be produced) to let the vacancies diffuse from there to the cell walls (where they are needed to assist climb and subsequent annihilation of cell wall with mobile dislocations). Therefore, the two dislocation characters can be treated in the same common framework in the present context. The common recovery term scales with the same annihilation length y_e=6b proposed by Essmann and Mughrabi [105],

$$\left(\frac{d\rho_w}{dt}\right)^{-} = -2y_e\rho_w \frac{\dot{\gamma}}{b} = -2y_e \frac{\rho_w}{n} n \frac{\dot{\gamma}}{b}, \quad (41)$$

for single slip as well as for multiple slip on n symmetrically activated slip systems.

3.2.3. Generation of partial disclination dipoles. The keystones of any dynamic model of fragmentation are the mechanisms of nucleation and growth of fragment boundary segments. In a disclination-based model, these mechanisms correspond to the elementary mechanisms of generation of partial disclination dipoles (PDD) and of propagation of partial disclinations (PD). Following subsection 2.2, the generation of a wedge PDD corresponds to the formation of a both-side terminating array of parallel excess edge dislocations of the same sign, or to the formation of two parallel semi-infinite walls of excess edge dislocations of opposite signs. The generation of a twist PDD corresponds to the formation of a both-side terminating net of two sets of parallel excess screw dislocations of the same sign, or of two parallel semi-infinite nets of parallel excess screw dislocations of opposite signs. A variety of different mechanisms was proposed to explain this nucleation of fragment boundary segments through collective behaviour of a couple of dislocations of the same sign [8,87,106-108]. The models suggested until 1960 [87,106] aimed at an understanding of nucleation of kink bands on the grain scale, the ones suggested later [107,108] were prompted by TEM observations of misorientation bands on the mesoscopic scale arising in stage III of plastic deformation [9,10,17].

From the beginning, two different routes were followed to explain kink banding on the grain scale and misorientation banding on the mesoscopic scale. On the one route, an *"imposed" macroscopic* background of kink band nucleation or a *grain-scale* background of misorientation band nucleation was suggested, e.g. constraints imposed by the holders [5] or stress concentrations at grain boundary ledges [108]. On the other route, an *"intrinsic" microscopic* background of kink band as well as misorientation band nucleation was proposed on the level of dislocation dynamics, namely collective behaviour or self-organization of dislocations.

Frank and Stroh [106] defined a kink band as a thin plate of sheared material in a non-sheared matrix, transverse to a slip direction and bounded by opposite tilt walls of dislocations (while in most of the later papers it was considered as a non-sheared plate in a sheared matrix). In such a configuration, the applied shear stress would drive the two opposite tilt walls not towards, but away from each other. Nevertheless, in case of finite tilt walls, the tips of the walls would still attract each other. Frank and Stroh determined the equilibrium between the repulsive force due to the external shear stress and the attracting force between the edges and calculated equilibrium band widths and lengths for parallel walls and for an elliptical band. Furthermore, an elliptical band with a sufficient angle of kinking could grow by generating new dislocation loops or pairs at its tips. The authors noted that the stress fields of kink bands were similar to those of slip bands, so that they "might act as sources for each other".

As already mentioned in subsection 1.1, Mader and Seeger [8] distinguished two different types of kink bands, one on the macroscopic scale arising already at the end of stage I and mainly in stage II

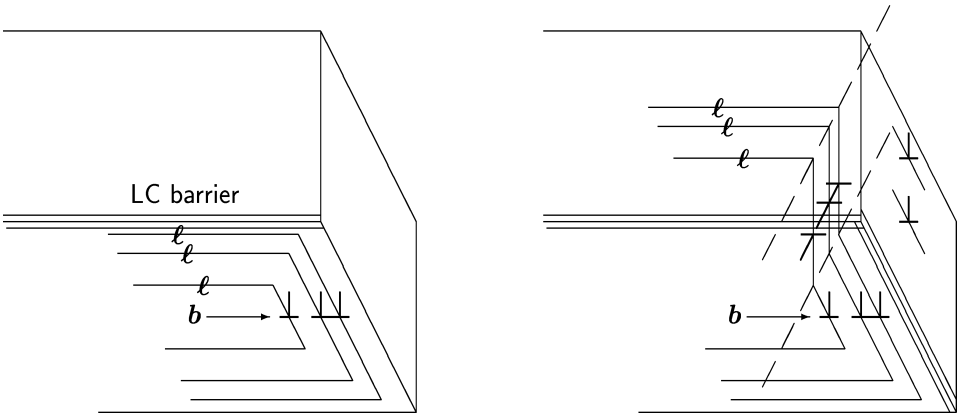

Fig. 9. Mechanism of kink band nucleation according to Seeger. To the left, piling-up of mobile dislocations at Lomer-Cottrell barriers limiting a glide zone. The glide zone is, for simplicity, sketched with a rectangular rather than with a hexagonal shape. To the right, the piled-up dislocations after cross-slip. Edge dislocations remaining in the primary slip planes can form nuclei of kink bands perpendicular to the primary slip plane. Edge dislocation segments remaining in parallel cross-slip planes can form nuclei of kink bands perpendicular to the cross slip plane.

(kink bands belonging to the deformation band structure in the terminology used in this paper) and one on the mesoscopic scale arising only in stage III (misorientation bands belonging to the fragment structure in the terminology used here). The onset of stage III is characterized by the resolved shear stress reaching a critical value to trigger off extensive cross-slip. Furthermore, the intensity of kink banding of the second type turns out to scale with the stacking fault energy. Therefore, cross-slip is most likely to be involved in misorientation banding.

Mader and Seeger suggested that cross-slip of screw dislocation segments piled-up at Lomer-Cottrell barriers would result in pairwise annihilation of screw segments from neighbouring glide zones leaving edge dislocations in the primary slip plane as well as edge segments in the cross slip planes behind (see Fig. 9). The glide motion of the primary edge dislocations could be hindered by Lomer-Cottrell barriers formed through reactions among secondary dislocations, and by the edge segments left behind in the cross-slip planes. On the one hand, the primary edges could then arrange in an energetically favourable wall configuration perpendicular to their slip plane. This both-side terminating wall might act as a nucleus of a kink band, and its stress fields might join the Lomer-Cottrell barriers in limiting the free path of the mobile dislocations. On the other hand, the edge segments in the cross-slip planes would always act as forest obstacles to the primary edges, but would, in general, not represent a low-angle grain boundary configuration. However, with the help of *Ergänzungsgleitung* (completion glide) [64,65], they could be completed to become a both-side terminating low-angle grain boundary. This could then limit the free path of the mobile dislocations in the slip direction and act as a nucleus of a second kink band.

Vladimirov [107] proposed a similar nucleation mechanism based on the redistribution of piled-up edge dislocations into an energetically favourable wall configuration with the help of vacancy-assisted climb. For such a mechanism, the intensity of misorientation banding should scale with the activation enthalpy of vacancy diffusion.

However, any mechanism based on impenetrable obstacles, e.g. Lomer-Cottrell barriers, can only explain the formation of *symmetric* kink bands or double walls with mutually compensating misorientations because the impenetrable obstacles also stop dislocations which travel in the opposite direction in the glide zone on the other side of the obstacle. In order to initiate the formation of an *asymmetric* kink band or double wall or a single wall with a non-vanishing total misorientation, either globally or locally *different slip rates on the two sides of the obstacle* are required. Since a negligible dislocation content of the cell interiors and an initially homogeneous orientation throughout the crystallite are assumed, there is no way to a *global* slip imbalance between the two sides of a cell wall (which would result in the formation of an excess dislocation layer on the cell wall in a straight-forward manner).

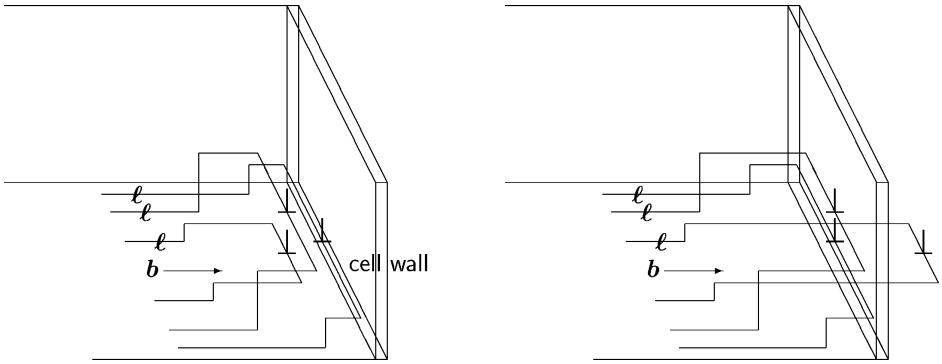

Fig. 10. Mechanism of fragment boundary nucleation used in the present model. On the left, double cross slip events in the cell interior resulting into bundles of mobile dislocations. The cross-slip planes are, for simplicity, sketched as perpendicular to the primary slip plane. To the right, the effect of a semi-transparent obstacle: some of the edge dislocations penetrate through the cell wall, others get stuck.

A *local* slip imbalance, however, can arise due to incidental *collective behaviour* of neighbouring mobile dislocations at a *semi-transparent obstacle* with *stochastic trapping*. If several neighbouring mobile dislocations approaching the cell wall incidentally all together get trapped, while their counterparts of opposite sign approaching the wall from the other side incidentally all together do *not* get trapped, then a both-side terminating excess dislocation wall representing a *nucleus of a fragment boundary* arises. Whether and on which conditions such a nucleus grows or gets "dissolved" again, will be discussed in the next subsection. As already pointed out by Pantleon [109], the semi-transparency of the obstacle and the stochastic character of the trapping process[1] thus are of crucial importance for misorientations to be formed. If the obstacle was an impenetrable one, then only a double excess dislocation wall with no net misorientation could be formed. If the trapping process would not have a stochastic character, incidental collective behaviour would not be possible and again only a double excess dislocation wall with no net misorientation would result.

As mentioned in subsection 1.1, Koneva, Kozlov and coworkes [38-40] proposed the coexistence of two fragment boundary nucleation mechanisms. In the first case, straight misorientation bands would be nucleated at grain boundary ledges and grow into the grain interior, in the second case disclination loops would be generated in the grain interior in the course of dislocation dynamics. The nucleation part of the first mechanism was recently modelled by Gutkin et al. [108] as a splitting event of partial disclinations in faults of grain boundaries triggered by the applied shear stress. The growth part of the first mechanism was already modelled by Romanov and Vladimirov [22] as propagation of partial disclination dipoles at the tips of the growing misorientation bands consisting of two parallel terminating excess dislocation walls with opposite signs. The present paper, on the contrary, focusses on modelling the second case, the nucleation and growth of loop-like fragment boundary layers on the grounds of dislocation dynamics.

As discussed in sections 2.1 and 3.1, the model presented in this paper starts from a well-developed cell structure, i.e. from a substructure which is typical for stage III of plastic deformation. Detailed light and electron microscopy studies of slip line patterns on the surface of deformed copper and aluminium single crystals [87,110] revealed already in the 1950s that during stage III the gliding dislocations get increasingly organized in *bundles* or *slip bands* and plastic deformation gets increasingly concentrated in the slip bands. This bundling or slip banding was attributed to extensive *double cross slip* [87,110-113]. Therefore, the model presented here assumes that the mobile dislocations are formed through double cross slip in the cell interiors and thus also supposes that they are grouped into bundles or slip bands (see Fig. 10).

In f.c.c. single crystals with intermediate and high stacking fault energy, there is a striking coincidence of
· the onset of massive cross-slip,
· the bundling of mobile dislocations in slip bands,

[1] Of course, this stochastic character of the trapping process is not a fundamental one, but just due to fluctuations in the dislocation structure of the cell wall and poor knowledge of its details.

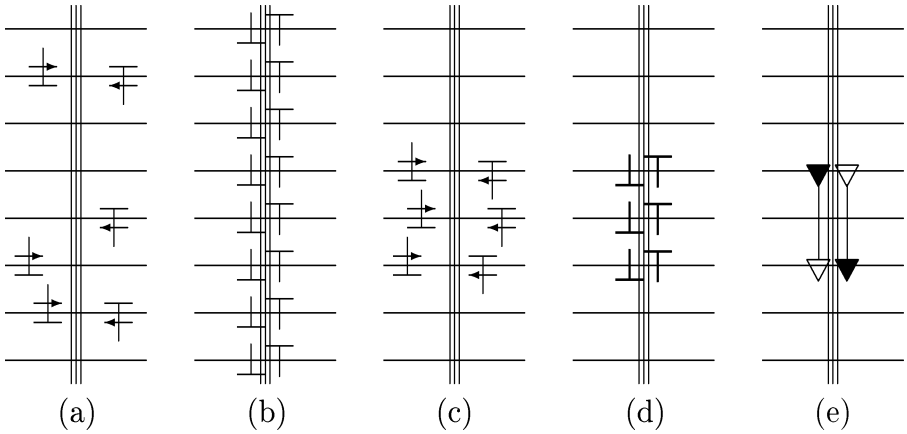

Fig. 11. Single-slip conditions: Generation of PDDs at semi-transparent obstacles. (a) balanced stopping of mobile dislocations, (b) double wall formed as a result of balanced stopping, (c) spatially non-balanced stopping of mobile dislocations, (d) both-side terminating double wall segment formed as a result of non-balanced stopping, (e) translation of (d) into disclination «language». Large edge symbols denote mobile, small ones redundant cell wall, bold ones non-redundant excess edge dislocations.

· the formation of a dislocation cell structure,
· and the onset of misorientation banding at the beginning of stage III.

If one takes into account that the mobile dislocations get bundled in slip bands in the course of stage III of plastic deformation (see the next subsubsection), one can use data from slip line measurements to estimate typical parameters of a partial disclination dipole representing a fragment boundary nucleus. Mader [114] studied low-symmetry oriented copper single crystals after tension at room temperature and found slip bands with 3-10 slip lines per band and lamella widths of about 300 Å. If one then assumes *incidental collective trapping* of the mobile dislocations in such a slip band at a cell wall, one gets an excess dislocation wall segment made up of $N \approx 5$ dislocations with an average spacing h of about 300 Å. This gives an initial PDD width of $2a_0 \approx 0.15$ μm and, according to Eq. (34), a misorientation of $\varphi \approx 0.085$. Müller and Leibfried [115] investigated low-symmetry oriented aluminium single crystals after tension at liquid air and at room temperature for a series of different strain rates. They found slip bands with 2-4 slip lines for $\dot{\varepsilon} > 10^{-2}\ s^{-1}$ at liquid air temperature and with 10-30 slip lines for $\dot{\varepsilon} < 10^{-2}\ s^{-1}$ and about 5 slip lines for $\dot{\varepsilon} > 10^{-2}\ s^{-1}$ at room temperature. The lamella widths were found around 700 Å at liquid air temperature and around 400 Å at room temperature, without clear dependence on the strain rate. This gives $2a_0 \approx 0.21$ μm and $\varphi \approx 0.0041$ for fast deformation at liquid air temperature, $2a_0 \approx 0.80$ μm and $\varphi \approx 0.0072$ for slow deformation at room temperature, and $2a_0 \approx 0.20$ μm and $\varphi \approx 0.0072$ for fast deformation at room temperature.

It has to be emphasized that slip line measurements do not provide any information about the *dynamics* of plastic deformation. Since the strain intervals used to generate the slip lines are rather large, one slip line can correspond to several mobile dislocations stepping out to the surface *at different times*. Consequently, the spacing between the slip lines does *not* equal the spacing between mobile dislocations arriving at an obstacle (perpendicular to the slip plane) *at the same time*. The spacings between collectively trapped dislocations derived above from the spacings between slip lines thus have to be considered as a *lower limit* or as a *rough aproximation*.

In order to obtain a *net* misorientation across the arising fragment boundary, it is of crucial importance that the excess dislocation layer on the one side of the cell wall does *not get compensated* by its counterpart with opposite sign on the other side of the cell wall (compare Figs. 11 and 12 below) - which is only possible for a *semi-transparent* obstacle with *stochastic* trapping. For a quantitative description of PDD generation through *incidental collective trapping* of mobile dislocations at cell walls, the two extreme cases of single slip (with cell walls roughly perpendicular to the slip plane, see Figs. 11 and 12) and of symmetric multiple slip (with cell walls bisecting the equivalent slip planes, see Fig. 13) are considered.

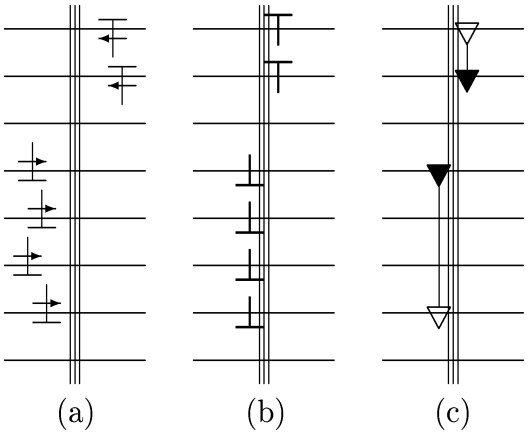

Fig. 12. Single-slip conditions: Generation of PDDs at semi-transparent obstacles. (a) spatially and directionally unbalanced stopping of mobile dislocations at a "hard" kinetic obstacle, (b) disordered excess dislocation wall formed as a result of non-balanced stopping, (c) translation of (b) into disclination "language". Large edge symbols denote mobile, small ones redundant cell wall, bold ones non-redundant excess edges.

The loss rate of mobile dislocations due to PDD generating trapping can be set up taking pattern from the loss rate due to ordinary trapping. The probability P_c of individual trapping in Eq. (40) has to be replaced by the probability $(P_c(1\text{-}P_c))^N$ of collective and non-compensated trapping of N dislocations. The probability product reflects the requirement that the trapped mobile dislocations must not be compensated by their counterparts of the opposite sign at the other side of the cell wall, the exponent reflects the collective behaviour of the N neighbouring mobile dislocations. In the case of single slip, one finds a generation rate for the (smeared-out) excess dislocation density of

$$\left(\frac{d\overline{\rho_{exc}}}{dt}\right)^{+} = -\left(\frac{d\rho_m}{dt}\right)^{-} = \frac{(P_c(1-P_c))^N f_{geom}}{Nd_c}\frac{\dot{\gamma}}{b} = \frac{(P_c(1-P_c))^N f_{geom}}{NK}\sqrt{\overline{\rho}_w}\frac{\dot{\gamma}}{b}. \tag{42}$$

The same collective trapping process occurs at fragment boundaries. The generation rate can be estimated taking patting from the one for the cell walls, but replacing the trapping probability P_c by the one P_f and replacing Holt's scaling law (32) for cells by the one (35) for fragments,

$$\left(\frac{d\overline{\rho_{exc}}}{dt}\right)^{+} = -\left(\frac{d\rho_m}{dt}\right)^{-} = \frac{(P_f(1-P_f))^N}{d_f}\frac{\dot{\gamma}}{b} = \frac{(P_f(1-P_f))^N}{166}\sqrt{\theta_i}\frac{\dot{\gamma}}{b}. \tag{43}$$

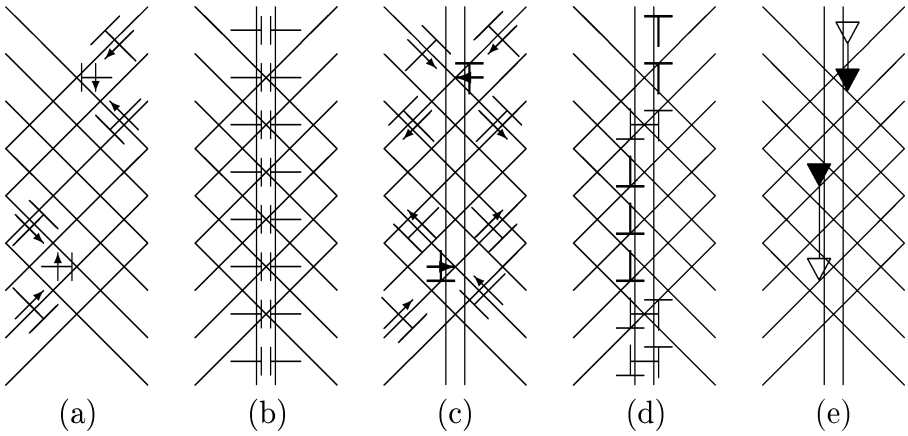

Fig. 13. Multiple-slip conditions: Generation of PDDs at cell walls. (a) formation of a cell wall through mobile dislocations either being stopped at a "hard" kinetic obstacle or interacting with each other to form non-glissile combined dislocations, (b) cell wall of the Mughrabi type, (c) cell wall as a glide obstacle triggering the storage of excess dislocations, (d) incidental irregularities in the dipolar character of the excess dislocation walls, (e) translation of (d) into disclination "language". Large edge symbols denote mobile, small ones redundant cell wall, bold ones non-redundant excess edges.

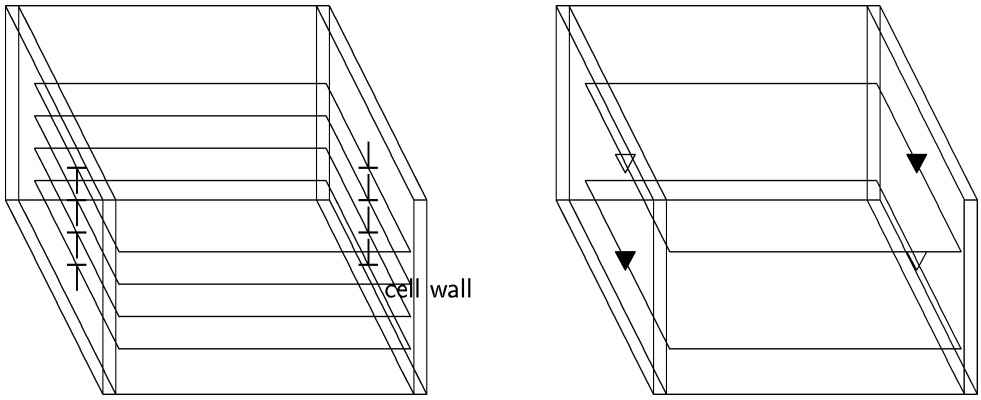

Fig. 14. Defect configuration resulting from fragment boundary nucleation. To the left, in the language of dislocations: a set of parallel dislocation loops along the cell wall obstacles. To the right, in the language of disclinations: a pair of parallel disclination loops at the border lines of the dislocation loop "cylinder" along the cell wall obstacles.

Since N collectively trapped mobile dislocations constitute one new partial disclination dipole, the corresponding PDD generation rate at cell walls reads

$$\left(\frac{d\theta_m}{dt}\right)^{+} = \frac{(P_c(1-P_c))^N f_{geom}}{Nd_c}\frac{\dot{\gamma}}{b} = \frac{(P_c(1-P_c))^N f_{geom}}{NK}\sqrt{\rho_w}\,\frac{\dot{\gamma}}{b}. \quad (44)$$

The major difference with the case of symmetric multiple slip is that the cell walls are not perpendicular then to the slip plane, but roughly bisecting the equivalent active slip planes (see Fig. 13). Consequently, neighbouring mobile dislocations from one slip system getting trapped collectively at a cell wall would not form a both-side terminating low-angle grain boundary configuration, so that *Ergänzungsgleitung* (completion glide) is required, or, more specific, mobile dislocations from the conjugate slip system are required to get trapped collectively as well and to react *formally* with the already trapped ones in order to form a low-angle grain boundary segment. As a result, collective behaviour of *twice as much* dislocations is required in the case of symmetric multiple slip which makes the probability of a PDD generating event dropping much below the probability in case of single slip. An example: If the individual trapping probability is $P_c = 1/3$, then the probability $(P_c(1\text{-}P_c))^{N=5}$ of collective and non-compensated trapping under single slip is about $5\cdot10^{-4}$, the probability $(P_c(1\text{-}P_c))^{N=10}$ of collective and non-compensated trapping under multiple slip is about $3\cdot10^{-7}$. While the first probability is already small, but still large enough to generate a sufficient density of partial disclinations fragmentating the crystallite, the second one turns out to be insufficient for fragmentation.

Since the long-range stress field around such a new PDD would drive the dislocation loop segments with the opposite sign at the other end of the loops away from the PDD and towards the neighbouring cell wall, a *local slip imbalance* would also be induced at this *neighbouring cell wall*. As a result, a loop-like fragment boundary layer as sketched in Fig.14 would form.

3.2.4.Propagation of partial disclinations. The conditions of growth of a finite excess edge dislocation wall through capturing and attaching additional excess dislocations were first discussed in the context of polygonization during recovery [66,73,74]. The total stress field of the finite dislocation wall was calculated as the sum of the stress fields of the individual dislocations. For the long-range stress field at large distances from the wall, the sum can be replaced by an integral. This gives a shear stress perpendicular to the wall of

$$\tau_{xy} = \frac{Gbx}{2\pi(1-\nu)h}\times\left(\frac{y+a}{x^2+(y+a)^2} - \frac{y-a}{x^2+(y-a)^2}\right), \quad (45)$$

where h is the dislocation spacing in the wall, $a = Nh/2$ denotes the half height of the wall, and the reference system is chosen as indicated in Fig.15.

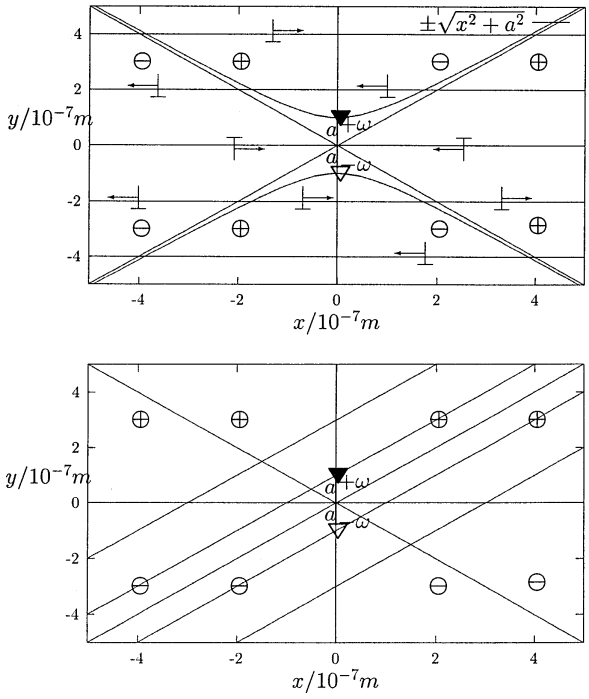

Fig. 15. "Capturing hyperbolae" above for single slip and below for multiply slip.

If one expresses the dislocation spacing through the misorientation according to Eq. (34), one finds the long-range stress field of the finite wall with dislocation spacing a and height $2a$ to be equivalent to the one of a partial disclination dipole with disclination strength $\omega = \varphi = b/h$ and dipole width $2a$,

$$\tau_{xy} = \frac{G\omega x}{2\pi(1-\nu)} \times \left(\frac{y+a}{x^2+(y+a)^2} - \frac{y-a}{x^2+(y-a)^2} \right). \quad (46)$$

As Nabarro showed already in 1952 [73], it follows from Eq. (45) that the finite wall or the PDD exerts an attracting Peach-Koehler force $F_x = b_x \tau_{xy}$ on an edge dislocation with matching sign inside the capture hyperbola (see Fig.15) given by

$$y_c^2 - x_c^2 = a^2. \quad (47)$$

However, the applied shear stress due to the finite wall or the PDD has to overcome the Peierls-Nabarro stress and the local effective shear stress, i.e. the external shear stress reduced by the mean internal shear stresses due to e.g. other dislocations or due to plastic strain or lattice rotation misfits,

$$\tau_{yx} > \tau_{PN} - \tau_{eff} = \tau_{PN} - \tau_{ext} + \tau_{int}. \quad (48)$$

Or, phrased in another way, the applied shear stresses due to the externally applied load and the PDD have to overcome the local shear resistance composed of the Peierls-Nabarro resistance and the shear resistance due to the current defect structure,

$$\tau_{yx} + \tau_{ext} > \tau^*_{PN} + \tau^*. \quad (49)$$

Determining the local internal and thus the local effective stress is a formidable task, so that in general strongly simplified representations of the defect structure are used to estimate the internal stress at least by order of magnitude. In the following, two rough estimations are carried out in order to find a minimum required partial disclination strength ω_p which allows PD propagation, i.e. PDD expansion or fragment boundary growth, and to find a capture length y_c, i.e. a distance ahead of a PD within which the PD is still able to capture a mobile dislocation of matching sign passing by.

From a graphical representation of the shear stress field τ_{xy} of a finite excess dislocation wall as shown by Li [74], one can read that the loop-shaped curves of attracting shear stresses of magnitude 0.3, 0.2 and 0.1 times a stress unit of $Gb/2\pi(1-\nu)h = G\varphi/2\pi(1-\nu)$, end up at distances of about 1.5, 2.5 and 5 times the wall half length a in front of the excess dislocation wall tip. In the case of, for instance, copper at room temperature this means

$$|\tau_{xy}(y = 5a)| < 0.1\frac{Gb}{2\pi(1-\nu)h} = 0.1\frac{G\varphi}{2\pi(1-\nu)} \approx 1000\varphi\,\text{MPa}. \quad (50)$$

A bundle of $N = 5$ dislocations with a slip plane distance of $h = 100b \approx 26$nm corresponding to a misorientation $\varphi = 0.01$ would then at $y = 5a$, i.e. at $4a \approx 0.26$ μm ahead of the wall tip, exert a shear stress of not more than 10 MPa (and of no more than 30 MPa at 0.5a=1.25h ahead of the wall tip). A group of $N = 5$ dislocations with $h = 1000$b ≈ 260 nm corresponding to $\varphi = 0.001$, however, would at $4a \approx 2.6$ μm ahead of the wall tip exert a shear stress of only less than 1 MPa (and of only less than 3 MPa at $0.5a=1.25h$ ahead of the wall tip). From this simple example, one can already guess that a partial disclination of strength $\varphi = \omega = 0.01$ would have a chance to grow by capturing additional mobile dislocations, whereas a partial disclination

of strength $\varphi = \omega = 0.001$ would not because the former would have a chance to overcome the local effective stress or the externally applied load plus the local shear resistance, whereas the latter would not.

For a quantitative evaluation of Eq. (49), the Peierls-Nabarro resistance is neglected for f.c.c. materials and the coordinates are rescaled in units of a to give $\tilde{x} = x/a$ and $\tilde{y} = y/a$, giving

$$\tau_{xy} = \frac{G\omega\tilde{x}}{2\pi(1-\nu)} \times \left(\frac{\tilde{y}+1}{\tilde{x}^2 + (\tilde{y}+1)^2} - \frac{\tilde{y}-1}{\tilde{x}^2 + (\tilde{y}-1)^2} \right). \quad (51)$$

The limiting curve where the applied shear stress due to the PDD equals the local effective stress is then defined by

$$\tilde{y}^4 - \frac{G\omega\tilde{x}}{\pi(1-\nu)\tau_{eff}}\tilde{y}^3 + 2(\tilde{x}^2 - 1)\tilde{y}^2 - \frac{G\omega(\tilde{x}^2-1)\tilde{x}}{\pi(1-\nu)\tau_{eff}}\tilde{y} + (\tilde{x}^2+1)^2 = 0. \quad (52)$$

A simple special case is $x = a$ or $\tilde{x} = 1$ giving

$$\tilde{y}^4 - \frac{G\omega}{\pi(1-\nu)\tau_{eff}}\tilde{y}^3 + 4 = 0. \quad (53)$$

To estimate the local effective stress, first consider an idealized framework of only the finite dislocation wall and a random distribution of mobile dislocations being present. Then the scaling law

$$\tau_{eff} = \alpha G b \sqrt{\rho_m} \quad (54)$$

proposed by Kocks, Argon and Ashby [84] for the local effective stress would apply. The mobile dislocation density ρ_m can be estimated from Orowan's law

$$\dot{\varepsilon} = m_s b \bar{v} \rho_m. \quad (55)$$

To estimate an average dislocation velocity in this context, one should better refer to the TEM in-situ measurements rather than to the pulse load and etching techniques because the continuous loading used in the in-situ tests is similar to the conditions of macroscopic straining [116]. In copper as well as in aluminium plastic deformation is carried out by few but fast mobile dislocations – Appel and Messerschmidt [117] measured an average dislocation velocity of $\bar{v} = 10^{-6}$ ms^{-1} in a TEM in-situ test on aluminium at room temperature. For a strain rate of $\dot{\varepsilon} = 10^{-2}$ s^{-1}, this gives a mobile dislocation density of about $\rho_m \approx 10^{14}$ m^{-2} which, according to Eq. (53), corresponds to an effective stress of about $\tau_{eff} \approx 20$ MPa. Inserting this into Eq. (52) gives two real roots of $y_{c,1} \approx 0.75a$ and $y_{c,2} \approx 10.2a$ for $\omega = 0.01$ and only complex roots for $\omega = 0.001$. An estimation of the capturing length carried out by the author [118] for the case of a PDD propagating at the top of a growing misorientation band also gave a capturing length of about $y_c \approx 10a$.

It can be concluded that the Peach-Koehler force exerted by a partial disclination with a strength beyond a required minimum strength of about $\omega_p = 0.01$ is sufficient to capture mobile dislocations passing by within a capturing length of about $y_c \approx 10a$, to attach them to the terminating excess dislocation wall and to let the partial disclination dipole expand. As Li [74] could show, such a process is also energetically feasible. It has to be emphasized that it is *only the bundling of slip in slip bands* which makes possible the nucleation of fragment boundary segments *that are able to grow*: this bundling in slip bands reduces the mean dislocation slip plane distance h in the slip bands of stage III compared to the one in the homogeneous fine glide regime of stage II, so that the resulting partial disclination strength exceeds the critical value of about $\omega_p = 0.01$. Thereby, slip banding and fragmentation, two different manifestations of collective behaviour in the dislocation ensemble, are closely related to each other.

The coupling of fragmentation to slip banding does not only lead to a minimum required disclination strength. Since the width of the lamellae between the slip lines in a slip band is only slightly changing in the further course of plastic deformation, it also offers an *average strength of a propagating partial disclination*, i.e. a *step-width of the increase in misorientation*. In this way, one can eliminate one of the parameters unknown in disclination in contrast to dislocation dynamics.

While Romanov and Vladimirov [22] "fed" the propagating partial disclination dipole at the top of a growing misorientation band by widening of dislocation loops from a static dislocation distribution between the two boundary planes ahead of the band tip, the present work follows a dynamic approach as proposed by Essmann and Mughrabi [105] in the context of dynamic recovery. The reasoning for a wedge PDD capturing a passing edge dislocation of the matching sign is exactly the same as for a cell wall edge dislocation spontaneously disintegrating with a passing edge dislocation of opposite sign (see subsection 3.2.2 and Fig. 16).

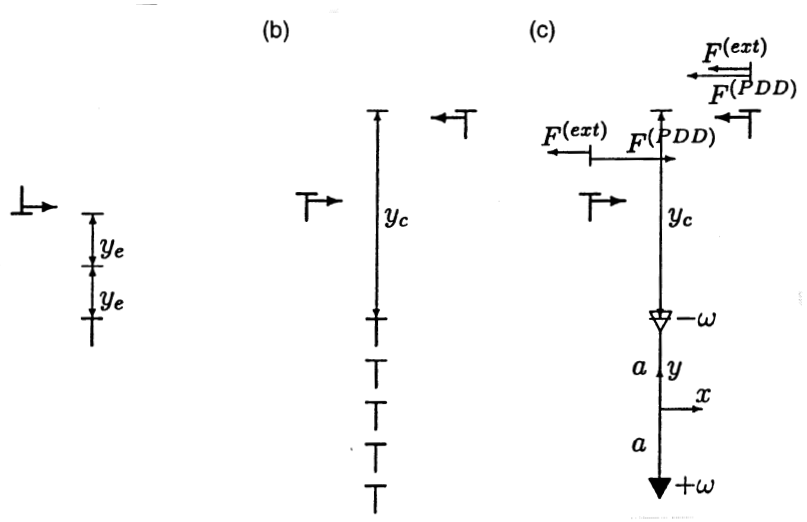

Fig. 16. a) Disintegration of an immobile edge dislocation with a mobile one of opposite sign passing by within the annihilation length y_e. b) Capture of a mobile dislocation passing by within the capturing length y_c ahead of the tip of a terminating excess dislocation wall (dislocation language). c) Capture of a mobile dislocation passing by within the capturing length y_c ahead of a partial disclination (the same in disclination language).

Formally, the density θ_p of dipoles of propagating partial disclinations replaces the density $\overline{\rho_w}$ of cell wall dislocations as sink density, and the capture length y_c replaces the annihilation length y_e,

$$\left(\frac{d\overline{\rho_{exc}}}{dt}\right)^{+} = -\left(\frac{d\rho_m}{dt}\right) = -2y_c\theta_p\frac{\dot{\gamma}}{b} = -20a_p\theta_p\frac{\dot{\gamma}}{b}, \tag{56}$$

where a_p denotes the average half width of the expanding dipoles of propagating partial disclinations.

The same mechanism, of course, also controls the mean *propagation speed* $\overline{V}$ of the partial disclinations: To calculate this velocity, one can estimate the time t_c which is needed by the mobile dislocation current $\dot{\gamma}/b$ to provide the N_c dislocations of the matching sign and character required by the PD to propagate by its own capturing length y_c,

$$t_c = \frac{N_c}{\frac{y_c}{4}\frac{\dot{\gamma}}{b}} = \frac{4\omega_p}{\dot{\gamma}}, \tag{57}$$

where Eq. (34) was used. This results in an average speed of

$$\overline{V} = \frac{y_c}{t_c} \approx \frac{10a_p}{4\omega_p}\dot{\gamma}. \tag{58}$$

3.2.5. Disclination storage: immobilization of propagating partial disclinations at fragment boundaries. For simplicity, it is assumed that each propagating partial disclination is definitely stopped at the next fragment boundary, i.e. in the next mesh of the fragment boundary mosaic (which is suggested by the analytical formula describing the interaction between a wide sessile and a narrow propagating PDD [23,119]). Then, the mean free path of a propagating PD equals the mean fragment size d_f, giving an immobilization term of

$$\left(\frac{d\theta_i}{dt}\right)^{+} = -\left(\frac{d\theta_p}{dt}\right)^{-} = \frac{1}{d_f}\frac{\overline{V}\theta_p}{2} = 0.602\sqrt{\theta_i}\frac{\overline{V}\theta_p}{2}, \tag{59}$$

where Eq. (35) was used. The factor of 1/2 is due to the transition from the *PD dipole* density θ_p to the *single PD* density θ_i. Note that the disclination immobilization term has the same structure as the dislocation storage term proposed by Kocks (cf. Eq. (9). Using expression (58) for the mean disclination speed finally gives

$$\left(\frac{d\theta_i}{dt}\right)^{+} = -\left(\frac{d\theta_p}{dt}\right)^{-} = 0.602\,\frac{10a_p b}{8\omega_p}\sqrt{\theta_i}\,\theta_p\,\frac{\dot{\gamma}}{b}. \quad (60)$$

3.2.6. An open question: disclination recovery. In order to study the substructural background of *stage V* of plastic deformation, one probably has to search for a mechanism of dynamic recovery of partial disclinations. A promising hint for such a mechanism might be the coupling between work-hardening in stage V and the hydrostatic pressure [120] because the wedge disclination density is also coupled to the hydrostatic stress [23]. Another possible mechanism might be the activation of additional slip systems around the PD triggered by their long-range stress fields. This would result in an accumulation of misfit-relieving dislocations around the PD, as proposed by Argon and Haasen for other sources of long-range stresses [58].

3.3. Substructure development

Collecting all the reaction terms from Eqs. (40), (41), (42), (43), (44), (56) and (60), transforming the evolution equations with the help of Orowan's law (m_S – Schmid factor)

$$\dot{\varepsilon} = m_S n b \bar{v} \rho_m \quad (61)$$

from the evolution parameter time to the evolution parameter strain and abbreviating all the reaction coefficients gives the following set of evolution equations:

$$\frac{d\overline{\rho_w}}{d\varepsilon} = I\sqrt{\overline{\rho_w}} - R\overline{\rho_w}, \quad (62)$$

$$\frac{d\overline{\rho_{exc}}}{d\varepsilon} = S_c\sqrt{\overline{\rho_w}} + S_f\sqrt{\theta_i} + E\theta_p, \quad (63)$$

$$\frac{d\theta_p}{d\varepsilon} = \frac{S_c}{N}\sqrt{\overline{\rho_w}} + \frac{S_f}{N}\sqrt{\theta_i} - J\sqrt{\theta_i}\,\theta_p, \quad (64)$$

$$\frac{d\theta_i}{d\varepsilon} = J\sqrt{\theta_i}\,\theta_p. \quad (65)$$

If one neglects collective trapping at cell walls compared to collective trapping at fragment boundaries, this system of ordinary differential equations has the advantage that the evolution equations (62) and (65) for the redundant dislocation density and the immobile partial disclination density which describe the substructure development and control the work-hardening can be solved analytically. Equation (62)) for the redundant dislocation density has the structure suggested by Mecking and Kocks [81] for the total dislocation density (cf. Eq. (10) in subsection 2.3) and can directly be integrated by separating the variables,

$$\overline{\rho_w}(\varepsilon) = \left(\frac{I - C_1 e^{-(\varepsilon-\varepsilon_y)/2}}{R}\right)^2. \quad (66)$$

The integration constant C_1 can be determined from the starting condition $\overline{\rho_w}(\varepsilon = \varepsilon_y) = \overline{\rho_w^0}$. The *stationary values* of the cell wall dislocation density and of the density of dipoles of propagating partial disclinations can directly be calculated and classified as *stable* stationary values:

$$\overline{\rho_w^s} = \left(\frac{I}{R}\right)^2 \quad \text{and}$$
$$\theta_p^s = \frac{S_f}{NJ}. \quad (67)$$

Inserting these stationary values into (64), one finds a simple law for the evolution of the slowly varying structure variable θ_i in the quasi-stationary state,

$$\left(\frac{d\theta_i}{d\varepsilon}\right)^{qs} = \frac{S_f}{N}\sqrt{\theta_i}, \quad (68)$$

or integrated (C_2 – integration constant)

$$\theta_i^{qs}(\varepsilon) = \left(\frac{S_f}{2N}\varepsilon + C_2\right)^2, \quad (69)$$

and through the relationship (35) also for the mean fragment size d_f:

$$\left(\frac{d\,d_f}{d\varepsilon}\right)^{qs} = -0.83\,\frac{S_f}{N}\,\frac{1}{\theta_i} = -0.30\,\frac{S_f}{N}\,d_f^2, \quad (70)$$

or integrated (C_3 – integration constant):

$$d_f^{qs}(\varepsilon) = \frac{1}{0.30(S_f / N)\varepsilon + C_3}. \quad (71)$$

Such a "hyperbolic" decrease matches with experimental observations [26].

The reaction coefficients R for dynamic recovery, E for capture of mobile dislocations through propagating partial disclination dipoles, and J for immobilization of propagating partial disclinations were calculated according to the expressions in (41), (56) and (60) with an annihilation length of $y_e = 6b$, a capturing length of $y_c = 10a$, an average width of

Table 2. Values of the reaction coefficients used in the model. Schmid factor m_s = 0.408.

coefficient	*value*	*reference*
I	$1.24 \cdot 10^9$ m^{-1}	fitting parameter for ξ = 0.20 [121], Eq. (40)
I	$8.29 \cdot 10^8$ m^{-1}	fitting parameter for ξ = 0.45 [55], Eq. (40)
R	29.4	Eq. (41)
E	$2.39 \cdot 10^4$	Eq. (56)
S_f	$3.83 \cdot 10^8$ m^{-1}	fitting parameter, Eq. (43)
J	$9.22 \cdot 10^{-4}$ m^{-1}	Eq. (60)

expanding partial disclination dipoles of $2a_p$ =0.1 μm, and a strength of the propagating partial disclinations of ω_p = 0.01, see Table 2. The reaction coefficients *I* for *"individual" trapping* of mobile dislocations in cell walls and S_f for *"collective" trapping* of mobile dislocations at fragment boundaries were used as *fitting parameters*. Their values were determined through fitting the modelled to an experimental flow curve for uniaxial compresssion of a [001]-oriented copper single crystal at room temperature, see Table 2.

The obtained values were then evaluated according to the expressions in (40), (42) and (43) with trapping probabilities of P_c = 1/3 at cell walls and P_f = 1/2 at fragment boundaries, a Holt constant of *K* = 16 and a geometric cell shape factor of f_{geom} = 2. The fitted coefficients then corresponded to a number *n* = 3 of locally active slip systems and to a number of *N* = 5 excess dislocations constituting a new partial disclination dipole. The first number corresponds to the experimental observation (cf., for instance, [58]) that, for symmetric orientations, usually much less than all the slip systems expected from a Schmid factor analysis (in this case eight) are locally activated. The second number corresponds well with the slip line measurements at the beginning of stage III as discussed in subsections 3.2.3 and 3.2.4.

The resulting *fragment size evolution* according to Eq. (35)) and the resulting *fragment misorientation evolution* according to Eq. (37) are displayed in Figs. 17 and 18. The results are in good agreement with the (rare) experimental data, see, for instance, [32,122].

3.4. Work-hardening

Fig. 19 displays the resulting *flow stress contributions* due to the cell structure or the redundant cell wall dislocations and due to the fragment structure

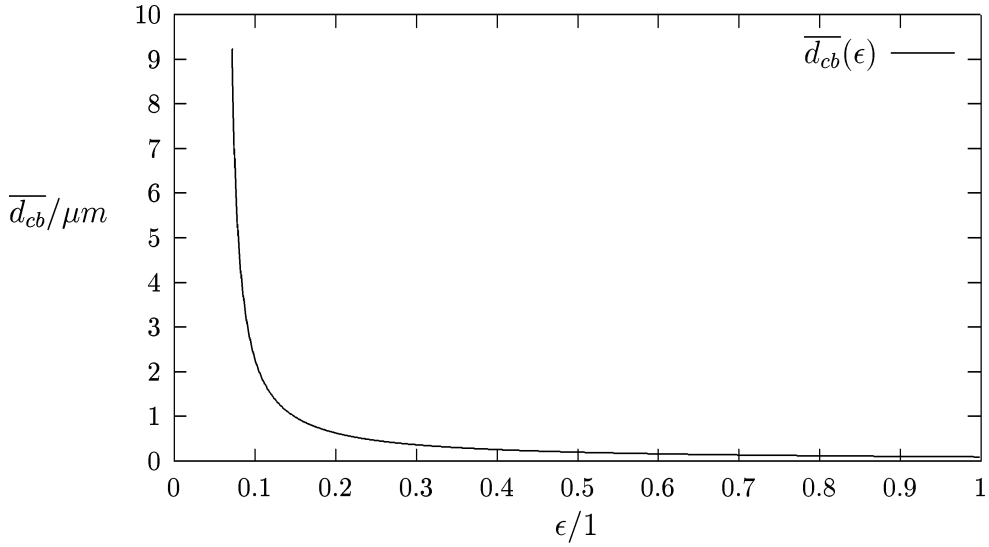

Fig. 17. Evolution of the mean fragment or cell block size with the (logarithmic) strain according to the simplified dislocation-disclination reaction kinetics model. Material parameters for copper, process parameters for room temperature and $\dot{\varepsilon} = 10^{-2}$ s^{-1}.

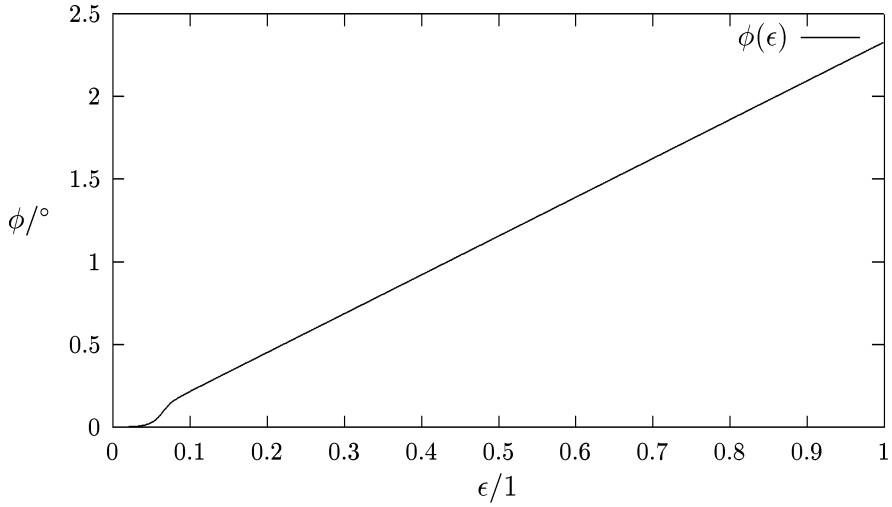

Fig. 18. Evolution of the mean misorientation across fragment or cell block boundaries with the (logarithmic) strain according to the simplified dislocation-disclination reaction kinetics model. Material parameters for copper, process parameters for room temperature and $\dot{\varepsilon} = 10^{-2}\ s^{-1}$.

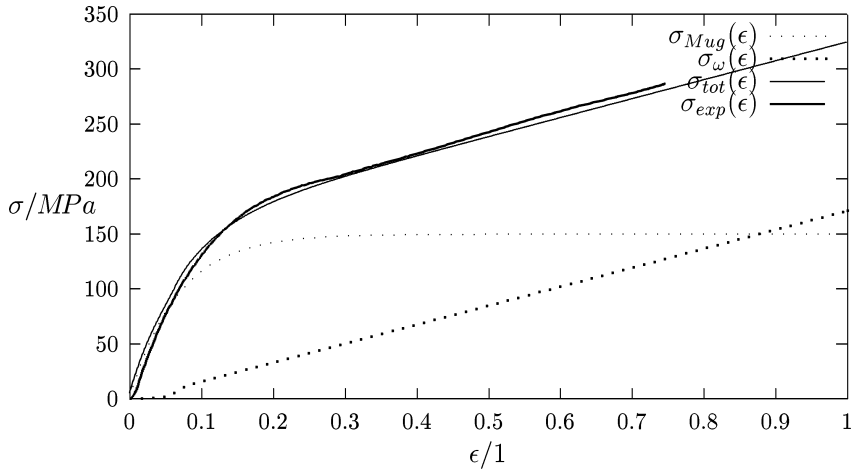

Fig. 19. Flow stress contributions of the redundant cell wall dislocation density and of the immobile partial disclination density and their sum according to the simplified dislocation-disclination reaction kinetics model. Trapping and cooperative trapping reaction coefficients I and S_f used as fitting parameters, Schmid factor $m_S = 0.408$, material parameters for copper, process parameters for room temperature and $\dot{\varepsilon} = 10^{-2}\ s^{-1}$. For comparison, the compression flow curve of a single crystal with highly symmetric orientation is shown.

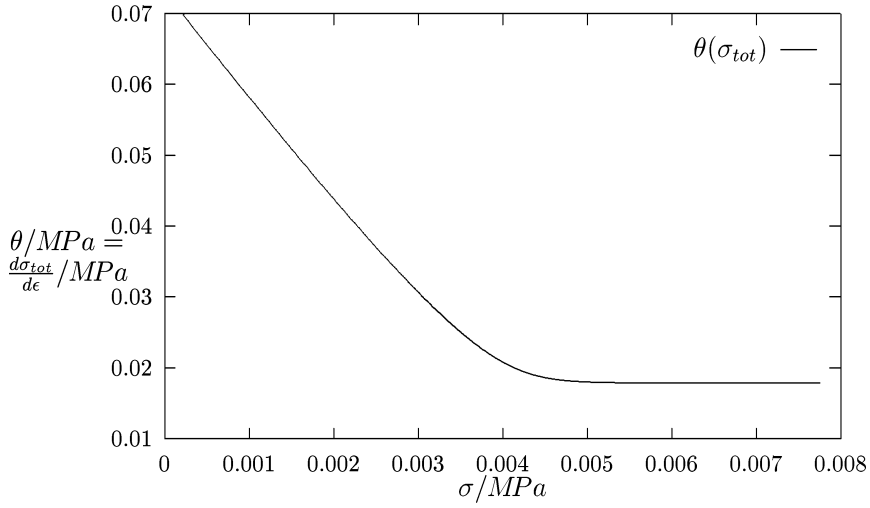

Fig.20. Kocks-Mecking plot corresponding to the modelled flow curve.

or the immobile partial disclinations in the fragment boundary triple junctions as well as the *total flow stress* according to Eq. (28). For comparison, an experimental flow curve from a uniaxial compression test at a [001] oriented copper single crystal at room temperature is also shown. In Fig. 20, the corresponding Kocks-Mecking plot is presented.

The stages III and IV of work-hardening can clearly be distinguished. *Stage III* can be attributed to the saturating local shear resistance of the *cell structure* due to the *redundant dislocations* in the cell walls. *Stage IV*, on the contrary, can be connected to the monotonously growing long-range internal stresses of the *fragment structure* due to the *immobile partial disclinations* in the fragment boundary triple junctions. This matches with the work-hardening concept presented by Kozlov, Koneva and coworkers [39-42].

ACKNOWLEDGEMENTS

The author wishes to thank P. Klimanek, Freiberg, and A.E. Romanov, St. Petersburg, for the introduction into the concept of disclinations and for continuous encouragement, support and help. W. Pantleon, Roskilde, V. Klemm, Freiberg, P. Van Houtte, Leuven, and E. Aernoudt, Leuven, contributed in many fruitful discussions to a critical and better understanding.

Financial support was given by the Deutsche Forschungsgemeinschaft (Graduate School "Physical Modelling in Materials Science") and the Fonds voor Wetenschappelijk Onderzoek – Vlaanderen (contract number G.0228.98).

REFERENCES

[1] E. Orowan // *Nature* **149** (1947) 643.
[2] A.S. Argon, In: *Physical Metallurgy*, 4th edition, ed. by R.W. Cahn and P. Haasen (North Holland, Amsterdam, 1996), vol. 3, p. 1877.
[3] C.S. Barrett and L.H. Levenson // *Trans. Amer. Inst. Min. Met. Eng.* **135** (1939) 327.
[4] C.S. Barrett and L.H. Levenson // *Trans. Amer. Inst. Min. Met. Eng.* **137** (1940) 112.
[5] R.W.K. Honeycombe // *J. Inst. Met.* **80** (1951-52) 49.
[6] R.W.K. Honeycombe // *J. Inst. Met.* **80** (1951-52) 45.
[7] W. Staubwasser // *Acta metall.* **7** (1959) 43.
[8] S. Mader and A. Seeger // *Acta metall.* **8** (1960) 513, in German.
[9] I.W. Steeds // *Proc. Roy. Soc. A* **292** (1966) 343.
[10] U. Essmann // *Phys. stat. sol.* **3** (1963) 932, in German.
[11] H. Mughrabi, In: *Constitutive Equations in Plasticity*, ed. by A.S. Argon (M.I.T. Press, Cambridge, MA, 1975), p. 199.
[12] H. Ahlborn // *Z. Metallkde.* **56** (1965) 205 and 411, in German.
[13] H. Ahlborn // *Z. Metallkde.* **57** (1966) 887, in German.
[14] H. Ahlborn and D. Sauer // *Z. Metallkde.* **59** (1968) 658, in German.
[15] A.S. Malin and M. Hatherly // *Met. Sci.* **13** (1979) 463.
[16] V.A. Likhachev and V.V. Rybin // *Izv. AN SSSR, ser. fiz.* **37** (1973) 2433, in Russian.
[17] A.S. Rubtsov and V.V. Rybin // *Fiz. met. metalloved.* **44** (1977) 611, in Russian.
[18] V.V. Rybin, *Bolshie plasticheskie deformatsii i razrushenie metallov (Large Plastic Deformations and Fracture of Metals)*, (Metallurgiya, Moskva, 1986), in Russian.
[19] F. Prinz and A.S. Argon // *Phys. stat. sol. (a)* **57** (1980) 741.
[20] V.I. Vladimirov and I.M. Zhukovskiy // Fiz. tverd. tela **16** (1974) 346, in Russian.
[21] V.A. Likhachev and V.V. Rybin // *Fiz. tverd. tela* **18** (1976) 163, in Russian.
[22] V.I. Vladimirov and A.E. Romanov // *Fiz. tverd. tela* **20** (1978) 3114, in Russian.
[23] A.E. Romanov and V.I. Vladimirov, In: *Dislocations in Solids*, vol. 9, ed. by F.R.N. Nabarro (North Holland, Amsterdam, 1992), p. 191.
[24] N. Hansen and D. Kuhlmann-Wilsdorf // *Mater. Sci. Engng.* **81** (1986) 141.
[25] B. Bay, N. Hansen, D. Hughes and D. Kuhlmann-Wilsdorf // *Acta metall. mater.* **40** (1992) 205.
[26] N. Hansen and D.A. Hughes // *Phys. stat. sol. (b)* **149** (1995) 155.
[27] Q. Liu and N. Hansen // *Phys. stat. sol. (a)* **149** (1995) 187.
[28] Q. Liu, D. Juul Jensen and N. Hansen // *Acta mater.* **46** (1998) 5819.
[29] D.A. Hughes and W.D. Nix // *Mater. Sci. Engng. A* **122** (1989) 153.
[30] D.A. Hughes and N. Hansen // *Mater. Sci. Technol.* **7** (1991) 544.
[31] D.A. Hughes and N. Hansen // *Acta mater.* **48** (2000) 2985.

[32] V.S. Ananthan, T. Leffers and N. Hansen // *Mater. Sci. Technol.* **7** (1991) 1069.
[33] A. Godfrey, D. Juul Jensen and N. Hansen // *Acta mater.* **46** (1998) 823.
[34] A. Godfrey, D. Juul Jensen and N. Hansen // *Acta mater.* **46** (1998) 835.
[35] Q. Liu and N. Hansen // *Proc. Roy. Soc. London A* **454** (1998) 2555.
[36] J.A. Wert, Q. Liu and N. Hansen // *Acta metall. mater.* **43** (1995) 4153.
[37] J. Weertman // *Scripta metall.* **20** (1986) 1483.
[38] N.A. Koneva, D.V. Lychagin, L.A. Teplyakova and L.I. Trishkina, In: *Disklinatsii i rotatsionnaya deformatsiya tverdykh tel (Disclinations and Rotational Deformation of Solids)*, ed. by V.I. Vladimirov and A.E. Romanov (Ioffe Physico-Technical Institute, Leningrad, 1988), p. 103, in Russian.
[39] N.A. Koneva, D.V. Lychagin, L.A. Teplyakova and E.V. Kozlov, In: *Proceedings of the 8th International Conference on the Strength of Metals and Alloys (ICSMA-8), Tampere, Finland, 22-26 August 1988, vol. 1*, ed. by P.O. Kettunen, T.K. Lepistö and M.E. Lehtonen (Pergamon, Oxford, 1989), p. 385.
[40] E.V. Kozlov, N.A. Koneva and L.I. Trishkina, In: *Disklinatsii i rotatsionnaya deformatsiya tverdykh tel (Disclinations and Rotational Deformation of Solids)*, ed. by V.I. Vladimirov and A.E. Romanov (Ioffe Physico-Technical Institute, Leningrad, 1990), p. 89, in Russian.
[41] E.V. Kozlov and N.A. Koneva // *Mater. Sci. Engng. A* **234-236** (1997) 982.
[42] E.V. Kozlov and N.A. Koneva, to be published in *Mater. Sci. Engng. A*, special issue (2001).
[43] L. Delannay, O.V. Mishin, D. Juul Jensen and P. Van Houtte // *Acta mater.* **49** (2000) 2441.
[44] C.S.Lee, B.J. Duggan and R.E.Smallman // *Acta metall. mater.* **41** (1993) 2265.
[45] T. Leffers // *Phys. stat. sol. (a)* **149** (1995) 69.
[46] T. Leffers // *Int. J. Plast.* **17** (2001) 469.
[47] T. Leffers // *Int. J. Plast.* **17** (2001) 491.
[48] H. Mughrabi // *Acta metall.* **31** (1983) 1367.
[49] F.B. Prinz and A.S. Argon // *Acta metall.* **32** (1984) 1021.
[50] W.D. Nix, J.C. Gibeling and D.A. Hughes // *Metall. Trans. A* **16** (1985) 2215.
[51] P. Haasen // *J. Physique* **50** (1989) 2445.
[52] M. Zehetbauer // *Acta metall. mater.* **41** (1993) 589.
[53] H. Mughrabi // *Mater. Sci. Engng.* **85** (1987) 15.
[54] J. Gil Sevillano, In: *Materials Science and Technology*, ed. by R.W. Cahn, P. Haasen and E.J. Kramer, vol. 6, *Plastic Deformation and Fracture of Materials*, ed. by H. Mughrabi (VCH, Weinheim, 1993), p. 19.
[55] E. Göttler // *Phil. Mag.* **28** (1973) 1057.
[56] H. Mughrabi, T. Ungár, W. Kienle and M. Wilkens // *Phil. Mag.* **53** (1986) 793.
[57] E. Schafler, M. Zehetbauer and T. Ungár, to be published in *Mater. Sci. Engng. A*, special issue (2001).
[58] A.S. Argon and P. Haasen // *Acta metall. mater.* **41** (1993) 3289.
[59] F.R.N. Nabarro // *Scripta metall. mater.* **30** (1994) 1085.
[60] A. Seeger and M. Wilkens, In: *Reinststoffprobleme, Bd. III: Realstruktur und Eigenschaften von Reinststoffen*, ed. by E. Rexer (Akademie-Verlag, Berlin, 1967), p. 29, in German.
[61] W. Pantleon, *Modellierung der Substrukturentwicklung bei Warmverformung (Modelling of Substructure Development during Hot Deformation*), *Freiberger Forschungshefte*, vol. B 280 (TU Bergakademie Freiberg, Freiberg, 1996), in German.
[62] B. Escaig, In: *Dislocation Dynamics*, ed. by A.R. Rosenfield, G.T. Hahn, A.L. Bement and R.I. Jaffee (McGraw-Hill, New York, 1968), p. 655.
[63] P.Paufler and G.E.R. Schulze, *Physicalische Grundlagen der mechanischen Festorpreigenshaften* (Academic-Verlag, Berlin, 1978), in German.
[64] H. Müller // *Z. Metallkde.* **50** (1959) 165, in German.
[65] H. Müller // *Z. Metallkde.* **50** (1959) 351, in German.
[66] F.R.N. Nabarro, *Theory of Crystal Dislocations* (Clarendon, Oxford, 1967).
[67] R. de Wit // *J. Res. Nat. Bur. Stand. (U.S.)* **77 A** (1973) 49, 359 and 607.
[68] V. Volterra // *Ann. Ecole Norm. Sup. Paris* **24** (3) (1907) 401.
[69] J.C.M. Li // *Surf. Sci.* **31** (1972) 12.
[70] J.C.M. Li, In: *The Nature and Behaviour of Grain Boundaries*, ed. by H. Hu (Plenum Press, New York, 1972), p. 71.
[71] A.E. Romanov // *Mater. Sci. Engng. A* **164** 58.

[72] A. Luft // *Solid State Phenomena* **23-24** (1992) 285.
[73] F.R.N. Nabarro // *Adv. Phys.* **1** (1952) 269.
[74] J.C.M. Li // *Acta metall.* **8** (1960) 563.
[75] V. Klemm, P. Klimanek and M. Seefeldt // *Bull. Czech Slovak Cryst. Assoc.* **5** (special issue) (1998) A 21.
[76] V. Klemm, P. Klimanek and M. Seefeldt // *Phys. stat. sol. (a)* **175** (1999) 569.
[77] A.N. Tyumentsev, M.V. Tretiak, A.D. Korotaev, Yu. P. Pinzhin, R.Z. Valiev, R.K. Islamgaliev and A.V. Korznikov, In: *Investigations and Applications of Severe Plastic Deformation*, *Proceedings of the NATO Advanced Research Workshop*, 2-7 August 1999, Moscow (Russia), ed. by T.C. Lowe and R.Z. Valiev, NATO Science Series 3. High Technology, vol. 80 (Kluwer, Dordrecht, 2000), p. 127.
[78] M. Seefeldt // *Mater. Phys. Mech.* **1** (2000) 54.
[79] W.G.Johnson and J.J. Gilman // *J. Appl. Phys*. **30** (1959) 129.
[80] U.F. Kocks // *Trans. ASME, J. Engng. Mater. Technol.* **98** (1976) 76.
[81] H. Mecking and U.F. Kocks // *Acta metall.* **29** (1981) 1865.
[82] A.N. Orlov // *Fiz. met. metalloved.* **20** (1965) 12, in Russian.
[83] G.A. Malygin // *Usp. Fiz. Nauk* **169** (1999) 979, in Russian.
[84] U.F. Kocks, A.S. Argon and M.F. Ashby, In: *Progress in Materials Science*, vol. 19, ed. by B. Chalmers, J.W. Christian and T.B. Massalski (Pergamon, Oxford, 1975), p. 1.
[85] P.B. Hirsch, In: *Internal Stresses and Fatigue in Metals*, ed. by G.M. Rassweiler and W.L. Grube (Elsevier, Amsterdam, 1959), p. 139.
[86] G. Saada, In: *Electron Microscopy and Strength of Crystals*, ed. by G. Thomas and J. Washburn (Interscience, New York, 1963), p. 651.
[87] A. Seeger, In: *Handbuch der Physik*, vol. VII/2, ed. by S. Flügge (Springer, Berlin, 1958), p. 1, in German.
[88] J.F. Nye // *Acta metall.* **1** (1953) 153.
[89] E. Kröner, *Kontinuumstheorie der Versetzungen und Eigenspannungen (Continuum Theory of Dislocations and Eigenstresses)* (Springer, Berlin, 1958), in German.
[90] M.F. Ashby // *Phil. Mag.* **21** (1970) 399.
[91] W. Pantleon and P. Klimanek, In: *Microstructural and Crystallographic Aspects of Recrystallization*, Proceedings of the 16th Risø International Symposium on Materials Science, Roskilde (Denmark), 4-8 September 1995, ed. by N. Hansen, D. Juul Jensen, Y.L. Liu and B. Ralph (Risø National Laboratory, Roskilde, 1995), p. 473.
[92] U.F. Kocks // *Metall. Trans.* **1** (1970) 1121.
[93] J. Gil Sevillano and F.J. Torrealda, In: *Deformation of Polycrystals: Mechanisms and Microstructures*, Proceedings of the 2nd Risø International Symposium on Materials Science, Roskilde, Denmark, 14-18 September 1981, ed. by N. Hansen, A. Horsewell, T. Leffers and H. Lilholt (Risø National Laboratory, Roskilde, 1981), p. 185.
[94] F.J. Torrealda and J. Gil Sevillano, In: Proceedings of the 6th International Conference on the Strength of Metals and Alloys (ICSMA-6), Melbourne, Australia, 16-20 August 1982, vol. 1, ed. by R.C. Gifkins (Pergamon, Oxford, 1983), p. 547.
[95] G. Saada and E. Bouchaud // *Acta metall. mater.* **41** (1993) 2173.
[96] G. Saada and D. Sornette // *Acta metall. mater.* **43** (1995) 313.
[97] J. Gil Sevillano, P. Van Houtte and E. Aernoudt // *Progr. Mater. Sci.* **25** (1980) 69.
[98] D.L. Holt // *J. Appl. Phys.* **41** (1970) 3197.
[99] M.R. Staker and D.L. Holt // *Acta metall.* **20** (1972) 569.
[100] S.V. Raj and G.M. Pharr // *Mater. Sci. Engng.* **81** (1986) 217.
[101] D. Stoyan, W.S. Kendall and J. Mecke, *Stochastic Geometry and its Applications*, 2nd edition (Wiley, Chichester, 1995).
[102] J. Ohser and U. Lorz, *Quantitative Gefügeanalyse (Quantitative Microstructure Analysis)*, *2nd edition, Freiberger Forschungsheft*, vol. B 276 (TU Bergakademie Freiberg, Freiberg, 1996), in German.
[103] M. Barthel, P. Klimanek and K.E. Hensger, *Czech. J. Phys. B* **38** (1988) 377.
[104] P. Ambrosi and C. Schwink // *Scripta metall.* **12** (1978) 303.
[105] U. Essmann and H. Mughrabi // *Phil. Mag. A* **40** (1979) 731.
[106] F.C. Frank and A.N. Stroh // *Proc. Phys. Soc. B* **65** (1952) 811.
[107] V.I. Vladimirov, *Einführung in die physikalische Theorie der Festigkeit* (VEB

Deutscher Verlag für Grundstoffindustrie, Leipzig, 1976), in German.
[108] M. Yu. Gutkin, A.E. Romanov and P. Klimanek, In: *Local Lattice Rotations and Disclinations in Microstructures of Distorted Crystalline Materials*, Proceedings of the International Workshop, Rauschenbach (Germany), 10-14 April 2000, ed. by P. Klimanek (Trans Tech, Zürich, 2001), in print.
[109] W. Pantleon // *Acta mater.* **46** (1998) 451.
[110] J. Diehl, S. Mader and A. Seeger // *Z. Metallkde.* **46** (1955) 650, in German.
[111] N.F. Mott // *Proc. Phys. Soc. B* **64** (1951) 729.
[112] G. Leibfried and P. Haasen // *Z. Physik* **142** (1955) 87, in German.
[113] H. Wiedersich // *J. Appl. Phys.* **33** (1962) 854.
[114] S. Mader // *Z. Physik* **149** (1957) 73.
[115] H. Müller and G. Leibfried // *Z. Physik* **142** (1955) 87, in German.
[116] H. Neuhäuser, In: *Dislocations in Solids*, vol. 6, ed. by F.R.N. Nabarro (North Holland, Amsterdam, 1983), p. 319.
[117] F. Appel and U. Messerschmidt // *Phys. stat. sol. (a)* **34** (1976) 175.
[118] M. Seefeldt, *Modellierung der Substrukturentwicklung bei Kaltumformung mit Hilfe von Disklinationen (Modelling of Substructure Development during Cold Deformation with the Help of Disclinations), Freiberger Forschungshefte, vol. B 304* (TU Bergakademie Freiberg, Freiberg, 2000), in German.
[119] V.I. Vladimirov and A.E. Romanov // *Fiz. tverd. tela* **26** (1984) 610, in Russian.
[120] J. Gil Sevillano and E. Aernoudt // *Mater. Sci. Eng*. **86** (1987) 35.
[121] M. Müller, M. Zehetbauer, A. Borbély and T. Ungár // *Z. Metallkde.* **86** (1995) 827.
[122] B.M. Bykov, B.A. Likhachev, Yu. A. Nikonov, L.L. Serbina and L.I. Shivalova // *Fiz. metall. metalloved.* **45** (1978) 163.